

An Exploration of Neural Oxygenation as a Function of Arterial Fluid Dynamics

Prepared By: Abigail Holland (20002693)

Prepared For: Biological Fluid Dynamics (MECH 461), Queens University

Date Submitted: April 20, 2020

Course Professor: Dr. Claire Davies

Data Collection Colleague: Amir Moslehi

Associated GitHub Software Found At:

[abbyholland/fnirs_analysis](https://github.com/abbyholland/fnirs_analysis) and [abbyholland/neural_fluid_dynamics](https://github.com/abbyholland/neural_fluid_dynamics)

Abstract

Neurological biometrics are used in the diagnosis of a myriad of neurological disorders, provide metrics for the creation of cognitive prediction models, and are essential to the development of human-machine interfaces. Commonly determined through non-invasive measurement techniques, neurological biometrics rely on oxygenation and blood volume level fluctuations over time in the brain. Differences in normal and hypertensive blood pressure conditions have been shown to change the pulsatile nature of cerebral arteries, as well as the oxygen flux through cerebral arterial walls. Understanding cerebral arterial fluid dynamics is essential to identify relationships present between oxygenation and blood pressure levels.

This paper provides a quantitative analysis of the effect of blood velocity and blood pressure on neural oxygenation levels through a theoretical model and empirical research.

The relationships between blood pressure, blood velocity and oxygen flux were empirically tested using male subjects in their early twenties. Additionally, the difference in oxygen flux across the motor imagery and motor execution trials was analyzed for possible trends.

Empirical research involved a participant wearing sensory equipment and performing simple hand movements as a response to stimuli. The motor execution experimental movements required the participants to squeeze either their left or right hand as directed by a left or right arrow stimulus presented on a screen. The experiment was repeated for motor imagery with the participants imagining the movements rather than actually performing them. The oxygenation levels were considered at resting state, as well as right and left responses for both the motor execution and motor imagery experiments.

Pilot data was collected from participants wearing an electroencephalogram (EEG) headcap with functional Near-Infrared Spectroscopy (fNIRS) capabilities. The headcap collecting fNIRS data was connected to the OXYMON software and the data was converted into a MATLAB data file for analysis. Blood pressure and other blood fluid properties were also collected using a blood pressure cuff and Photoplethysmogram (PPG) during the pilot phase. Unfortunately, the COVID-19 protocols required that the hospital-based lab be closed eliminating the opportunity to use a finger- attached plethysmography sensor to collect additional data. With lab access, the blood pressure cuff and plethysmography sensor would be connected to the BIOPAC software and separately recorded. Two lab technicians are required to successfully run the experiment.

The collected empirical results were compared against a model created from externally produced simulated arterial blood flow data to confirm the model's accuracy. The associated theoretical model was developed using MATLAB to calculate fluid properties including blood velocity, arterial wall shear stress, and oxygen saturation using simulated normal and hypertensive blood pressure condition data. The main theoretical and empirical comparison would include respective trend analysis of wall shear stress and the percentage of oxygenated hemoglobin, both as a function of continuous blood pressure.

As a complete data set was not retrieved, the focus of this paper involves the procedure, set-up, and theoretical analysis of data collected. Going forward, data collection using this procedure will be essential to drawing empirical conclusions about the relationship between blood pressure, blood volume, and the percentage of oxygenated hemoglobin. As well, assessing the larger data set will enable a more definitive opinion on the accuracy of the theoretical MATLAB model.

Table of Contents

Abstract	2
Table of Figures	5
List of Tables	6
1.0. Introduction	7
2.0. Background Knowledge	8
2.1. Neuroscience Research Methods	8
2.2. Neural Fluid Dynamics	9
2.3. Arterial Hypertension	9
3.0. Theoretical Model	10
3.1. Relevant Neuroanatomy	10
3.2. Considered Variables	11
3.3. Model Assumptions	12
3.4. Theoretical Results	12
3.5. Theoretical Model Discussion	14
4.0. Empirical Testing Overview	15
4.1. Procedure Outline	15
5.0. Data Collection	17
5.1. Data Inaccuracies Resulting from Halted Testing	17
5.2. Functional Near-Infrared Spectroscopy Data	18
5.3. Blood Pressure Data	20
5.4. Photoplethysmogram Data	21
6.0. Developed Empirical Analysis Software	22
6.1. Software Structure and Capabilities	22
6.2. Analysis Potential	23
7.0. Signal Filtering, Manipulating, and Processing	23
7.1. Manual Functional Near-Infrared Spectroscopy Data Manipulations	23
7.2. Functional Near-Infrared Spectroscopy Data Filtering	26
7.3. Photoplethysmogram Data Filtering	27
8.0. Applied Calculations	27
8.1. Photoplethysmography Calculations	27
8.2. Blood Pressure Calculations	29
8.3. Functional Near-Infrared Spectroscopy Calculations	29
8.4. Functional Near-Infrared Spectroscopy Averaged Values	32

Abigail Holland	Exploration of Cerebral Arterial Fluid Dynamics
9.0. Expected Analysis	34
9.1. State Comparison Analysis	34
9.2. Action Comparison Analysis	38
9.3. Participant Comparison Analysis	40
9.4. Static Blood Pressure Impact Analysis	42
9.5. Continuous Blood Pressure Trend Results	46
10.0. Theoretical and Empirical Comparison	47
11.0. Acknowledgements	47
12.0. Conclusion	47
Bibliography	49
Appendix A: Theoretical Methods and Model	52
Model Specifications	52
Flow Properties	52
Velocity Calculations	53
Appendix B: Additional Graphs	54
fNIRS Averaged Values	54
Action Comparison Analysis	55
Static Blood Pressure Impact Analysis	57

Table of Figures

Figure 1: Pressure as a Function of Timestep for Basilar Artery and Posterior Cerebral Artery.....	12
Figure 2: Volumetric Flow as a Function of Timestep for Basilar Artery and Posterior Cerebral Artery.....	13
Figure 3: Shear Stress on the Wall as a Function of Timestep for Basilar Artery and Posterior Cerebral Artery.....	13
Figure 4: Velocity as a Function of Diameter for the Posterior Cerebral Artery under Normal and Hypertensive conditions.....	14
Figure 5: Velocity as a Function of Diameter for Basilar Artery and Posterior Cerebral Artery under Normal and Hypertensive conditions.	14
Figure 6: The electroencephalogram headcap used for functional Near-Infrared Spectroscopy data collection and the associated functional Near-Infrared sensors.	16
Figure 7: The Artinis Medical System used for functional Near-Infrared Spectroscopy data collection.....	17
Figure 8: Participant 1 Motor Imagery Filtered Data Depicting Oxygenated Hemoglobin Concentration.	18
Figure 9: Participant 1 Motor Imagery Filtered Data Depicting Deoxygenated Hemoglobin Concentration.	19
Figure 10: Blood Pressure Testing Data.	21
Figure 11: Photoplethysmogram Testing Data.....	22
Figure 12: Participant 2 Motor Imagery Filtered and Unmanipulated Data Depicting Oxygenated Hemoglobin Concentration.	24
Figure 13: Participant 2 Motor Imagery Filtered and Manipulated Data Depicting Oxygenated Hemoglobin Concentration.	25
Figure 14: Participant 2 Motor Imagery Filtered Data Depicting Oxygenated Hemoglobin Concentration Only edited for Corruption.	26
Figure 15: Participant 2 Motor Imagery Filtered and Unfiltered Data Depicting Oxygenated Hemoglobin Concentration.	27
Figure 16: Photoplethysmogram Data Including Identified Peaks.	28
Figure 17: Photoplethysmogram Data Derived Twice.	29
Figure 18: Participant 1 Motor Imagery Filtered and Manipulated Data Depicting Oxygenated Hemoglobin Concentration and Deoxygenated Hemoglobin Concentration and Blood Volume for Channel 1.....	30
Figure 19: Participant 1 Motor Imagery Filtered and Manipulated Data Depicting the Percentage of Oxygenated Hemoglobin Concentration for Channel 1.	31
Figure 20: Participant 1 Motor Imagery Filtered and Manipulated Data Depicting the Percentage of Oxygenated Hemoglobin Concentration for Channel 1 with the Applied Moving Average Filter Edits.	32
Figure 21: Participant 1 Motor Imagery Filtered and Manipulated Data Depicting the Averaged Epoch for Blood Volume for the Relevant Channels of each State: Rest, Right, and Left.	33
Figure 22: Participant 1 Motor Imagery Filtered and Manipulated Data Depicting the Averaged Epoch for the Percentage of the Oxygenated Hemoglobin Concentration for the Relevant Channels of each State: Rest, Right, and Left.	34
Figure 23: Participant 1 Motor Imagery Filtered and Manipulated Data Depicting the Averaged Epoch Oxygenated Hemoglobin Concentration for the Relevant Channels of the Right and Left States as a Function of the Rest State.	35
Figure 24: Participant 1 Motor Imagery Filtered and Manipulated Data Depicting the Averaged Epoch Deoxygenated Hemoglobin Concentration for the Relevant Channels of the Right and Left States as a Function of the Rest State.	36
Figure 25: Participant 1 Motor Imagery Filtered and Manipulated Data Depicting the Averaged Epoch Blood Volume for the Relevant Channels of the Right and Left States as a Function of the Rest State.	37

Figure 26: Participant 1 Motor Imagery Filtered and Manipulated Data Depicting the Averaged Epoch for the Percentage of Oxygenated Hemoglobin Concentration for the Relevant Channels of the Right and Left States as a Function of the Rest State.....	38
Figure 27: Participant 1 Filtered and Manipulated Averaged Blood Volume Epoch for the Relevant Channels of the Differences between the Motor Imagery and Motor Execution Data for Each State.....	39
Figure 28: Participant 1 Filtered and Manipulated Averaged Percentage of Oxygenated Hemoglobin Concentration Epoch for the Relevant Channels of the Differences between the Motor Imagery and Motor Execution Data for Each State.....	40
Figure 29: Filtered and Manipulated Motor Imagery Trial Blood Volume Data Averaged Epoch for the Relevant Channels Depicting the Difference Between Each Participant for Each State.....	41
Figure 30: Filtered and Manipulated Motor Imagery Trial Percentage of Oxygenated Hemoglobin Data Averaged Epoch for the Relevant Channels Depicting the Difference Between Each Participant for Each State.....	42
Figure 31: Filtered and Manipulated Motor Imagery Trial Blood Volume Data Averaged Epoch for Every Relevant Channel for the Rest State for Both Participants.	43
Figure 32: Filtered and Manipulated Motor Imagery Trial Blood Volume Data Averaged Epoch for Every Relevant Channel for the Right State for Both Participants.	44
Figure 33: Filtered and Manipulated Motor Imagery Trial Percentage of Oxygenated Hemoglobin Data Averaged Epoch for Every Relevant Channel for the Rest State for Both Participants.	45
Figure 34: Filtered and Manipulated Motor Imagery Trial Percentage of Oxygenated Hemoglobin Data Averaged Epoch for Every Relevant Channel for the Right State for Both Participants.	46
Figure 35: Participant 1 Motor Imagery Filtered and Manipulated Data for Summarized and Averaged Epochs for Percentage of Oxygenated Hemoglobin Concentration and Blood Pressure for Trend Analysis.....	47
Figure 36: Participant 1 Motor Imagery Filtered and Manipulated Data Depicting the Averaged Epoch for Oxygenated Hemoglobin Concentration for the Relevant Channels of each State: Rest, Right, and Left.	54
Figure 37: Participant 1 Motor Imagery Filtered and Manipulated Data Depicting the Averaged Epoch for Deoxygenated Hemoglobin Concentration for the Relevant Channels of each State: Rest, Right, and Left.	55
Figure 38: Participant 1 Filtered and Manipulated Averaged Oxygenated Hemoglobin Concentration Epoch for the Relevant Channels of the Differences between the Motor Imagery and Motor Execution Data for Each State.....	56
Figure 39: Participant 1 Filtered and Manipulated Averaged Deoxygenated Hemoglobin Concentration Epoch for the Relevant Channels of the Differences between the Motor Imagery and Motor Execution Data for Each State..	57
Figure 40: Filtered and Manipulated Motor Imagery Trial Blood Volume Data Averaged Epoch for Every Relevant Channel for the Left State for Both Participants.	58
Figure 41: Filtered and Manipulated Motor Imagery Trial Percentage of Oxygenated Hemoglobin Data Averaged Epoch for Every Relevant Channel for the Left State for Both Participants.	59

List of Tables

Table 1: Global variables used throughout the model.....	11
Table 2: ADAN Table of Pressure values [21].	11
Table 3: fNIRS Channel Descriptions.	19

1.0. Introduction

This research paper focuses on the fluid dynamics of cerebral arterial blood flow. Specifically, this report aims to model how blood flows through neural blood vessels and to empirically test the relationships between blood pressure, blood volume, and arterial oxygen flux.

Conducting explorations into the relationships between these properties is essential to growing academia's comprehension of neural properties and fluid-based neuroscience and therefore improving our understanding of how the brain functions. Understanding the functionality of the brain is essential to understanding what causes neurological disorders and how to cure these disorders or to mitigate their symptoms.

Neurological disorders affect hundreds of millions of people and account for 12 percent of global deaths [1]. In addition to fatalities, neurological disorders have a large impact on the quality of life for those suffering from the disorders. Neurological disorders can affect people of any age, region, or income level, and is an affliction relevant to all societies. With so many of the population affected by neurological disorders, and with such a detrimental impact on health and quality of life, understanding, mitigating, and symptom alleviation of neurological disorders is a priority for many health organizations. Successfully resolving neurological disorders, however, requires a more comprehensive understanding of the complexities of the brain than experts have today.

The brain is an extremely complicated biological system that top neuroscientists still fail to fully comprehend. Each area of neuroscience has significant opportunity for growth and the development of new ideas. Many forms of non-invasive neuroscience analysis methods rely directly on measuring fluid flow through the brain. Neurological biometrics are often gathered using the measurement of blood volume, oxygen concentrations, and blood pressure in certain sections of the brain over time. Analyzing the dynamics of neural fluid flow is useful in understanding brain function under different contexts. Accurate models of fluid dynamics affecting both oxygen and blood pressure have the potential to greatly improve neuroscience analysis.

The theoretical model described in this paper will use these relationships to produce a largely conceptual model which aims to highlight the impact of pressure changes on brain activation. Brain activation levels are directly linked to the amount of oxygen delivered to neural cells through blood flow. Oxygenation is quantifiably measured by considering the oxygen flux through blood vessel walls. Oxygen flux, as well as the shear stress acting along the vessel wall, has been found to be directly impacted by the velocity of the blood [2] [3]. In blood vessels, pressure directly impacts blood velocity throughout the cardiac cycle.

The empirical testing discussed in this paper considers the relationship between blood pressure, blood volume, and the percentage of oxygenated hemoglobin. These physiological properties are compared by collecting participant data of males between the ages of 19 and 22 using a blood pressure cuff, a Photoplethysmography (PPG) sensor, and a functional Near-Infrared Spectroscopy (fNIRS) sensor. The collected and considered variables in analysis will include static and continuous blood pressure, oxygenated and deoxygenated hemoglobin concentrations, and heart rate metrics such as identified systolic peaks.

To limit potential confounding factors, both the theoretical model and empirical testing will assess normal and hypertensive blood pressure conditions. Arterial hypertension is a condition in which the participant presents consistently high blood pressure. The symptoms of arterial hypertension include headaches, fatigue, and weakened vision: all neurological symptoms. The condition of arterial hypertension has also shown to have a direct link to neurological disorders. This report will analyze the relationships of the aforementioned blood volume and oxygenated hemoglobin concentration and will use the comparison results of normal and hypertensive conditions to mitigate potential confounding factors.

The overall hypothesis investigated is that blood pressure conditions such as hypertension will directly impact properties relevant to cerebral fluid dynamics including blood volume, the percentage of oxygenated hemoglobin, and blood velocity.

2.0. Background Knowledge

This section will provide significant background on the relevance of this model and experiment to neuroscience, as well as background on the relevant anatomical and fluid dynamics.

2.1. Neuroscience Research Methods

There are myriad non-invasive neuroscience research methods which directly rely on neural fluid flow. These analysis methods rely on the coupling of cerebral blood flow and neuronal activation: activation in an area of the brain is directly and consistently linked to increased blood flow in that region [4]. This connection occurs as more activity requires more oxygen and produces more waste. As blood transports both waste and oxygen, blood flow is increased in these active areas. As the activity occurring in a section of the brain increases, the need for oxygen increases as well. The oxygen is transported in blood through the hemoglobin in capillary red blood cells. The magnetic characteristics of hemoglobin are quantifiable and dependent on whether or not they carry oxygen.

Functional Near-Infrared Spectroscopy (fNIRS) is one research method reliant on this aforementioned neuro-vascular coupling [5]. The fNIRS technique measures physiologic changes and is directly reliant on the fluid dynamics of neural blood flow [6]. The technique is used to interpret changes in intensity of neural activity throughout different regions of the brain. However, the levels of oxygenation measured by the fNIRS data collection and analysis methods have many limitations and potentially confounding factors due to complexity in structural neurology [7].

fNIRS uses infrared light analysis to measure hemodynamic responses in a specific area [8] [9]. The fNIRS system measures the hemoglobin by considering the properties of light before and after it is reflected off blood flowing through the brain at a specific point [10]. Oxygenated and deoxygenated hemoglobin have different absorption levels, enabling the analysis of oxygen consumption in the considered brain region over time [11]. One advantage of using fNIRS is that data is provided for a specific point in the brain rather than providing metrics on the entire brain.

Infrared technology can also be used to measure comparable fluid properties at a different physiological location that is both less expensive and easier to conduct due to simpler equipment. Photoplethysmography (PPG) sensor data is often measured non-invasively on the tip of the participant's index finger and can produce both relative blood fluid properties and heart rate metrics [12]. Blood volume and identified systolic peak calculated from the PPG data can be used as an individual analysis technique or in conjunction with another technique such as the fNIRS system described above for additional analysis potential.

A blood pressure cuff is a technique which can be used to measure static or continuous data describing the blood pressure of the participant. This cuff is simply applied to the participant's bicep and can be used individually to describe a participant's blood pressure or to supplement and support data collected from other measurement techniques.

In order to study oxygenation levels, the above fluid dynamic measurements and analysis techniques were used to limit the study variables to only blood vessel diameter and blood pressure. The model created for this paper focuses on two blood vessels with varying sizes under normal and heightened pressure conditions. The designed empirical experiment includes data collected using the aforementioned measurement techniques and focuses on

participants from a small age bracket of a single sex and a similar environment in an aim to decrease additional neurological variables.

These hemodynamic metrics can give insight into the structure and functionality of the brain which can be used in neural modelling, psychology, and neuroscience research. The changes in these measurements over time can also be correlated to specific metrics. As a participant's age, emotional context, and environment changes, their measured neural activity can also shift [8]. As oxygenation is used to research brain activation and functionality under different participant conditions, it is extremely important to understand how neural fluid dynamics affect cerebral blood flow with a particular focus on measured oxygenated hemoglobin. If cerebral blood flow can be modelled and accounted for, potential confounding factors could be eliminated, and neuroscientists can have a better understanding of controls and variables throughout the experimental process.

2.2. Neural Fluid Dynamics

Researchers at Leeds Beckett University, the University of Bradford and the Don Carlo Gnocchi Foundation have recently investigated how blood flows through the brain [7]. This group was able to track blood flow as a function of pressure shifts and map the flow of blood into and out of the brain. As blood is pumped from the heart through the brain, the blood moves into cranial arteries, through the brain, and exits through cerebral veins which follow the spinal cord anteriorly through the body [7]. As blood pressure changes, the cranial arteries contract and expand in a pulsating motion to move the blood throughout the brain at a steadier rate. With high blood pressure, the arteries expand and temporarily store blood. As the heart relaxes the blood pressure decreases and the cranial arteries contract in response which pushes the stored blood through the capillaries into the brain. The cerebral veins then expand to store the blood that is leaving the brain with this added capillary pressure. The cerebral veins, however, cannot store as much blood as the cranial arteries. This difference in capacity causes a pressure gradient and some of the cerebrospinal fluid in the cerebral veins flow back into the brain which produces a negative volumetric flow of blood. Each artery and vein in this system are consistently pulsating and dependent on each other. An increase in pressure such as experienced from arterial hypertension in any vein or artery system would disrupt the overall blood flow and disrupt the "normal" transportation of oxygen through the body as well as through the arterial walls. Recent neuroscience research investigates abnormal fluid behavior in terms of relationships between blood flow behavior and neurological disorders [13]. Over time the flexibility of blood vessels decreases which may additionally affect the fluid behaviors of blood flow over time [7]. This conducted research, as well as my produced model, show that neural fluid dynamics must be considered in neuroscience research.

The report summarized and discussed above outlines how fluid dynamics contribute to neural functioning. These research conclusions, and the model completed in this report, provide conceptual confirmation of the contribution fluid dynamics makes to oxygenation and cognitive functionality.

2.3. Arterial Hypertension

Arterial hypertension is the medical condition of consistent high blood pressure. Systole and diastole are respectively the processes of the heart muscle contracting and relaxing to apply positive and negative pressure gradients [14]. The heightened blood pressure metric consists of a systolic peak above 130 or a diastolic peak above 140. Arterial hypertension is a large cause of fatality with half a million deaths in the United States in 2017 resulting from hypertension as a primary or contributing cause [15]. Additionally, hypertension is linked to neurological diseases so each disorder group may be contributing to the intensity of participant conditions, with hypertension impacting neurological disorder participants and neurological conditions worsening hypertensive participant conditions.

Hypertension has been shown to damage blood cells and affect the flexibility of pulsating arteries [16]. As discussed in 2.2. Neural Fluid Dynamics, cerebral arterial flexibility is essential to healthy oxygen transport and blood flow. Hypertension both contributes to vascular dementia and increases the risk of cognitive impairment. Finally, antihypertensive therapies have shown to decrease the risk of dementia by 55% [16]. Therefore, arterial hypertension has been statistically and qualitatively proven to have a connection with neurological disorders and conditions. The quantified connection of the direct relationship between blood pressure, cerebral blood flow and arterial oxygen flux are still unknown. This exploration aims to quantify and numerically describe the conceptually proven connections.

3.0. Theoretical Model

The following theoretical model was developed using MATLAB software and aims to represent cerebral fluid dynamics and relationships from continuous blood pressure data. As it is extremely difficult to measure continuous cerebral fluid data using non-invasive techniques, this model relies on simulated data.

The background research outlines the direct role which understanding cerebral fluid dynamics plays in developing a greater understanding of neurological disorders. As brain activation levels have shown to be directly linked to oxygenation levels, this project aims to model oxygenation levels as a function of cerebral fluid properties. Since oxygen flux is directly proportional to wall shear stress, a more mathematically reliable fluids property, this model produces wall shear stress values under varying artery pressures and diameters to describe oxygen flux. This model additionally considers the direct relationship between blood pressure and blood velocity for increased insight into the relationships between the relevant fluid dynamics properties. Separately considering the blood pressure and blood velocity relationship produced in the code in comparison to the proven direct relationship confirms the modelled qualitative trends [17]. For accuracy, the model must consider the effect of both blood pressure and artery pulsation throughout the cardiac cycle.

The developed model requires an input of varying pressure values collected at set time intervals throughout the cardiac cycle. At each time step, the model produces new pressure values which reflect the pulsatile artery, the velocity fields throughout a simulated grid of the artery, the wall shear stress, and the volumetric flow. The model was applied to the basilar artery and posterior cerebral arteries under both normal and hypertensive conditions. The cardiac cycle produced for the model first reaches systole at a model timestep range of 5-10 and then transitions to diastole at a range of 20-25.

The model specifications and calculations are presented in more detail in Appendix A: Theoretical Methods and Model.

3.1. Relevant Neuroanatomy

Memory loss is a common symptom of neurological disorders which has been shown to be impacted by arterial hypertension [18] [19]. Therefore, only a few arteries which are relevant to memory will be directly considered for the theoretical model developed. Focusing the modelled analysis will allow for more constant conditions across which to test the hypothesis.

Blood enters and exits the brain through two major systems: the carotid arteries and the vertebral arteries. From these arteries, blood travels into many arteries with smaller diameters. As the vertebral arteries lead to the limbic system, this report will focus on the blood flow from the vertebral arteries to the limbic system, which includes the organs most relevant to the creation and storage of memory. The vertebral arteries combine in the basilar artery which breaks off into the posterior cerebral arteries which leads to the limbic system [18].

The basilar and posterior cerebral arteries were considered in the model to analyze trends in arterial oxygenation flux as a function of pressure.

3.2. Considered Variables

The global variables used throughout this model are shown in the table below [19] [20]:

Table 1: Global variables used throughout the model.

Global Variables	Definition
rho	Fluid density of blood [kg/m^3] [19]
mu	Dynamic viscosity of blood [Pa*s] [20]
freq	Frequency of the cardiac cycle for ADAN [cycles/s]

Highly accurate empirical evidence is extremely difficult to achieve for deep neural arteries due to the large amount of material the signals must propagate through. As there has not been much research conducted on blood pressure and cerebral fluid dynamics, the effect of blood pressure on the fluid-based measurement techniques is largely unknown. Instead of using potentially inaccurate empirical data, the Anatomically Detailed Arterial Network (ADAN) model was used [21]. The Anatomically Detailed Arterial Network is a model developed using average (male) arterial vasculature to simulate 1-Dimensional blood flow. The ADAN model produces the mean arterial pressure for each time value considered throughout the cardiac cycle.

The empirically determined average diameter dimensions cited in the ADAN for the Basilar Artery and the Posterior Cerebral Artery are respectively 3.448 mm and 1.633 mm. The pressure amplitudes produced from the ADAN model for each artery under both normal and hypertensive conditions were recorded at a timestep of 0.1 seconds for the cardiac cycle.

Table 2: ADAN Table of Pressure values [21].

Time [s]	Basilar Artery Normal Pressure [mmHg]	Basilar Artery Hypertensive Pressure [mmHg]	Posterior Cerebral Artery Normal Pressure [mmHg]	Posterior Cerebral Artery Hypertensive Pressure [mmHg]
0.0	75	120	75	115
0.1	70	115	70	110
0.2	120	175	110	170
0.3	110	180	105	175
0.4	110	175	105	170
0.5	95	160	94	160
0.6	100	150	96	150

0.7	95	140	90	140
0.8	85	130	85	125
0.9	80	125	80	120
1.0	75	115	75	115

3.3. Model Assumptions

The following assumptions regarding the blood vessels were considered throughout model analysis:

- The blood vessel remains at a constant averaged diameter;
- The fluid density and dynamic viscosity of blood is constant;
- The blood itself is incompressible;
- There is a no slip boundary condition at the walls of the artery; and
- Heat exchange between different parts of the cardiovascular flow and nearby bodies was assumed negligible.

3.4. Theoretical Results

The pressure is presented below as a function of time for the Basilar Artery and the Posterior Cerebral Artery under both normal and hypertensive conditions. Under both normal and hypertensive conditions, pressure shifts over time as a function of the cardiac cycle between positive and negative values as expected from anatomical theory. The modelled pressure values under hypertensive conditions follow the same trend as normal conditions yet have more extreme values at systole and diastole. This produced simulation is flawed however, as arterial hypertension is consistently a higher blood pressure and the produced pressure values generated for the hypertensive conditions are more extreme than normal, not consistently higher. Although the produced values for each artery are similar, the Basilar Artery had higher pressure values produced under both normal and hypertensive conditions.

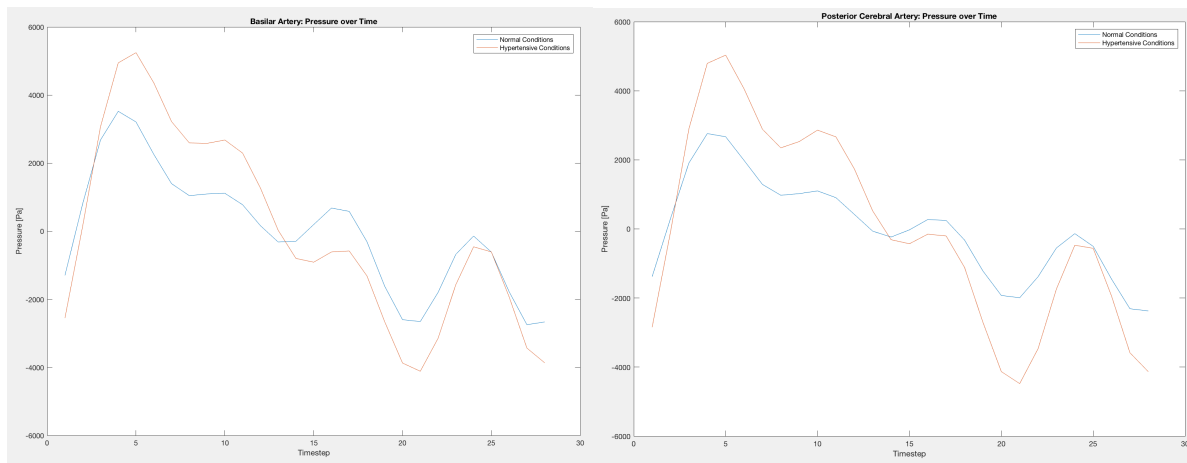


Figure 1: Pressure as a Function of Timestep for Basilar Artery and Posterior Cerebral Artery.

The volumetric flow rate for the Basilar Artery under normal and hypertensive conditions follow a similar pattern but are differentiated in terms of maxima and minima. Again, the hypertensive conditions display exaggerated

results at the trough and peaks when compared to the normal volumetric flow pattern. The larger maxima and smaller minima are a rational response to increased pressure during the diastole and systole, respectively. The basilar artery is shown to have more volumetric flow throughout both conditions, as can be seen in the difference of axis scales in the figures produced below. Additionally, the volumetric flow in the posterior artery is found to produce more negative values than those simulated for the basilar artery. Similar to the modelled pressure results, the volumetric flow produced for both arteries display more extreme systolic and diastolic values for the hypertensive conditions.

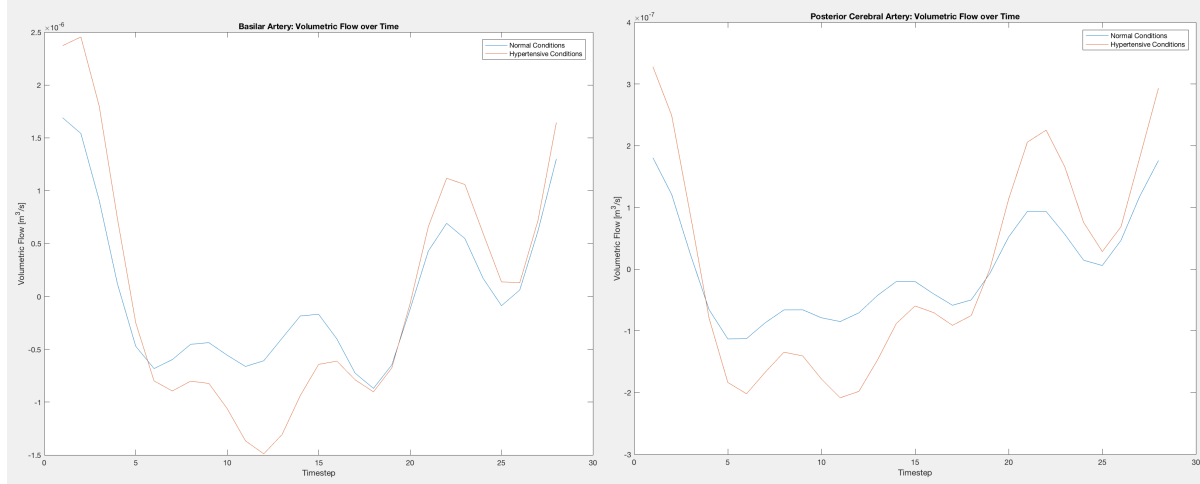


Figure 2: Volumetric Flow as a Function of Timestep for Basilar Artery and Posterior Cerebral Artery.

The shear stress acting on the wall throughout the cardiac cycle for both considered arteries is strongest at systole and reaches a local minimum at diastole. Under hypertensive conditions, the shear stress acting on the arterial wall is stronger throughout systole and applies stronger negative pressure during diastole. The shear stress acting on the arterial wall experienced on the wall also differs throughout the different arteries. The systolic hypertensive values for the posterior cerebral artery have two local maxima which imply heightened shear stress acting on the wall in comparison to the normalized conditions as well as the hypertensive basilar artery values.

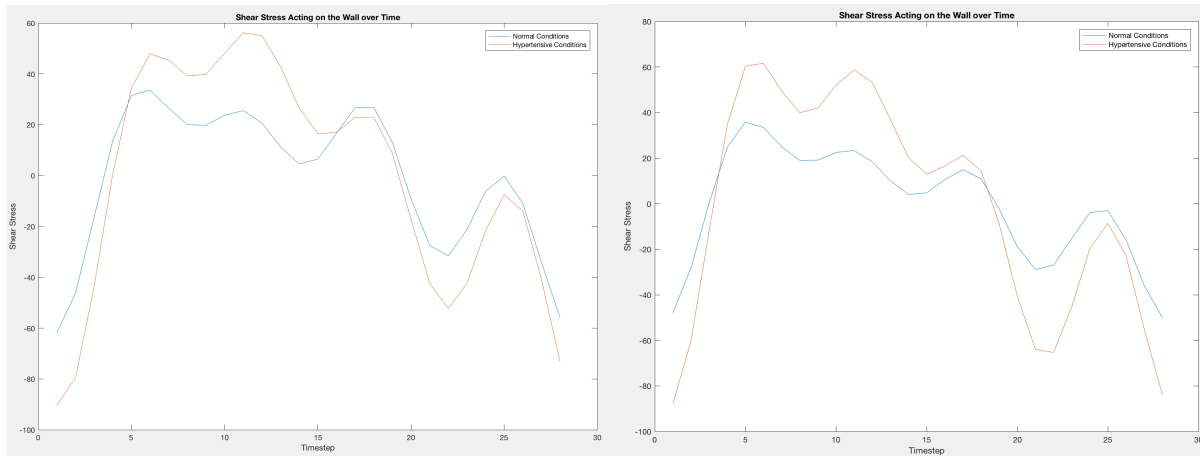


Figure 3: Shear Stress on the Wall as a Function of Timestep for Basilar Artery and Posterior Cerebral Artery.

The flow velocity profiles presented in the graphs below represent the velocity in terms of the artery radius for each timestep considered. The maximum velocity achieved by the hypertensive conditions was 0.12 m/s, which is

significantly greater than the 0.08 m/s maximum velocity under normal conditions. The flow characteristics show that throughout systole the flow velocity increases, reaches fully developed flow, then decreases. During diastole the flow has a negative velocity as it slows under the negative pressure conditions.

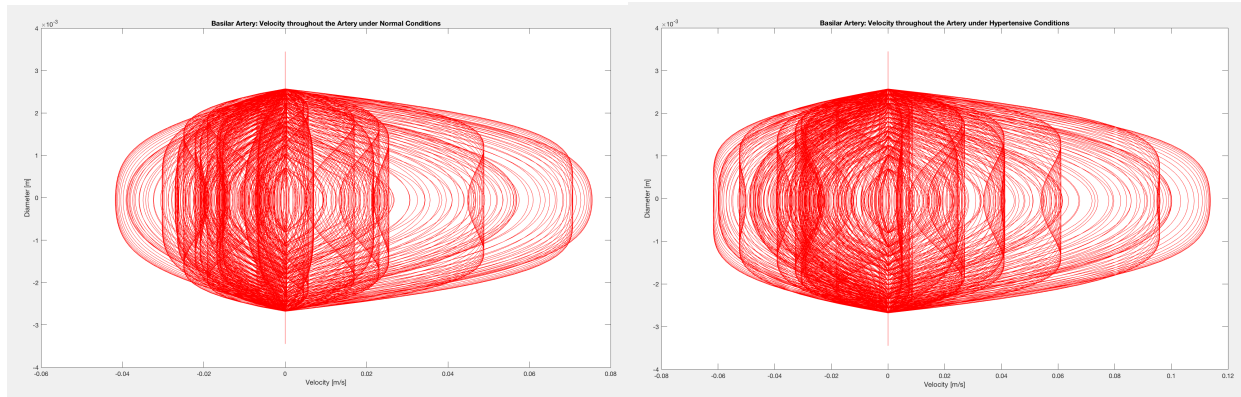


Figure 4: Velocity as a Function of Diameter for the Posterior Cerebral Artery under Normal and Hypertensive conditions.

The velocity presented in the posterior cerebral artery model similarly shows larger velocities reached under hypertensive conditions. Additionally, these conditions show faster achievement of flow development where the velocity profile is flat for a very short period of time before the flow becomes more circular. This circular behavior likely results from a decrease in pressure following systole.

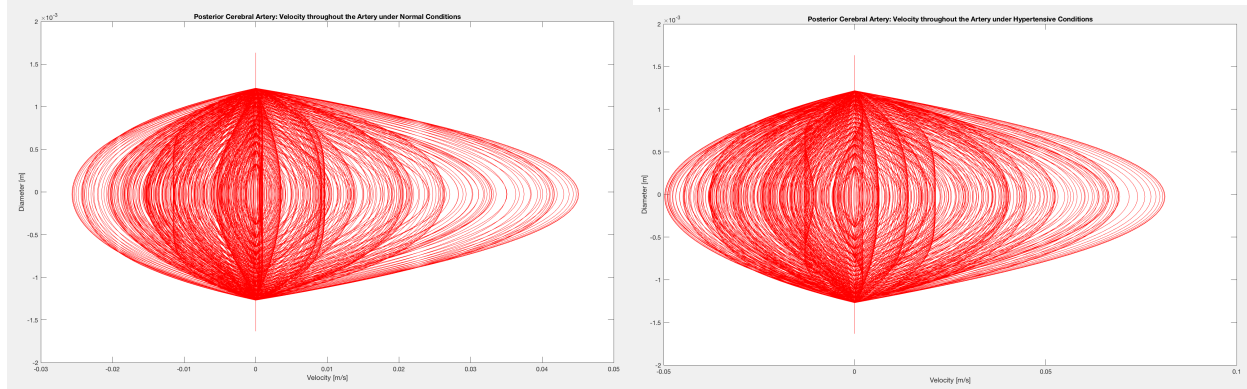


Figure 5: Velocity as a Function of Diameter for Basilar Artery and Posterior Cerebral Artery under Normal and Hypertensive conditions.

3.5. Theoretical Model Discussion

The produced model had considerable limitations and should be considered in terms of qualitative results rather than quantitative values. The ADAN neural artery simulated pressure values were not empirically proven and therefore could be inaccurate. Although the ADAN simulation has been empirically tested throughout other parts of the body, the implicit invasiveness of measuring neural arteries makes it a research field with very limited empirical data. This uncertainty may contribute to improper results throughout the model.

As the ADAN data used in this analysis was 1-Dimensional, the consideration of vorticity throughout the artery was not considered in this model. It is known from the research discussed in 2.2. Neural Fluid Dynamics that neural cell transport is directly impacted by the size and state of the blood vessel. Additionally, the clinical analysis discussed analyzes the results of increased or decreased vorticity at the arterial wall. Going forwards the model could be

improved in accuracy by mathematically considering how diffusion and increased blood flow affects cell oxygenation and waste transport. In future iterations of this model 2-Dimensional pressure values would enable analysis of vorticity and would increase the accuracy of the wall shear stress values produced. The combination of considering produced vorticity and diffusion in addition to the large-scale pressure changes would aid in improving the accuracy of this neural arterial model.

The shear stress acting on the wall over time was calculated as wall shear stress can qualitatively approximate oxygen flux as both properties are directly proportional to increased blood velocity. Existing research conducted on measuring oxygen flux is very limited and not supported with significant empirical evidence. Rather than add further potential inaccuracies, the oxygenation of the artery was instead conceptually related to the shear stress on the wall. The shear stresses produced throughout the cardiac cycle were then compared to reflect the probable patterns in oxygen flux. The results produced from this model demonstrated that oxygen flux varies widely throughout the cardiac cycle. Particularly, the wall shear stress graphs produced highlight the volatile results produced under hypertensive conditions. This disparity of high blood pressure relative to normal conditions confirms the hypothesis that shifts in pressure greatly affect the produced oxygen flux. Additionally, these results confirm that the effect of physiological fluid dynamics conditions such as hypertensive blood pressure conditions must be considered as a relevant factor in assessing cognitive functioning and in neurological analysis methods.

Additional studies conducted at the University of Pohang in the Republic of Korea analyzed the fluid dynamics present in blood vessels in a clinical study [21]. It was found that swirling blood flow has beneficial effects on blood circulation through blood vessels due to enhanced cross-plane mixing of the blood. With increased movement in the fluid flow, the blood better communicates with the cells. Blood vessels with larger diameters and under increased pressure conditions were reported to increase the development of vortices occurring near the arterial wall. This increased development of vortices was found to directly enhance the mixture of blood flow and oxygen delivery. This additionally confirms the effect fluid dynamics can have on the transport of oxygen and waste disposal throughout the brain. Including vorticity in future iterations of this model would add accuracy and strength to the conclusions drawn from the analysis of the model.

4.0. Empirical Testing Overview

The approach to this empirical experiment included the following steps in the required order of completion:

- designing the experiment including test design, target data, and required equipment;
- develop and test a software package for interpreting and analyzing data;
- conducting the experiment including recruiting participants and collecting data; and
- drawing conclusions from the graphical trends.

Unfortunately, COVID-19 protocols were imposed limiting access to the hospital-based lab where the experiment was to be conducted. As a consequence, only the design phase and software development phase were completed. In the absence of empirical data from test participants, graphical displays and illustrative trends were developed using pilot data recorded from 2 fNIRS participant datasets and 1 PPG and blood pressure participant dataset.

4.1. Procedure Outline

The relationship between blood pressure, blood velocity and oxygen flux were empirically tested using light-skinned, male subjects in their early twenties. This target group of males in their early twenties was chosen specifically to limit the confounding factors associated with age and gender [22]. A consistent participant skin

colour, described generally above as light-skinned, was selected as skin pigmentation affects the tissue oxygen saturation levels read with fNIRS devices [23].

The conducted test involved motor imagery and motor execution experimentation that varied trial conditions to allow for multiple analysis scenarios. The experimental procedure involved a participant wearing sensory equipment and performing simple hand movements as a response to stimuli. The motor execution experimental movements the participants were instructed to do were squeezing either their left or right hand as directed by a left or right arrow stimulus presented on a screen. The experiment was repeated for motor imagery with the participants instead imagining the movements rather than performing the tasks. The oxygenation levels were considered for resting states, as well as right and left responses for both the motor execution and motor imagery experiments. The motor imagery and execution experiments will allow for comparative analysis conditions as the experiment is theoretically identical with the exception of physical movements in the motor execution trials [24]. With only one variable, changes in blood pressure and oxygen flow associated with minor physical movements are easily considered and quantified [25].

Throughout experimentation, the participant wore an EEG headcap with fNIRS capabilities, a blood pressure cuff, and a finger-attached plethysmography sensor. The EEG cap held the fNIRS recording sensors and allowed the sensors to be placed in consistent locations across various participants. Both the EEG cap and the fNIRS recording sensors can be seen in the figure below. The fNIRS sensors used in this experiment included eight split transmitters, which each transmit two signals at different wavelengths.

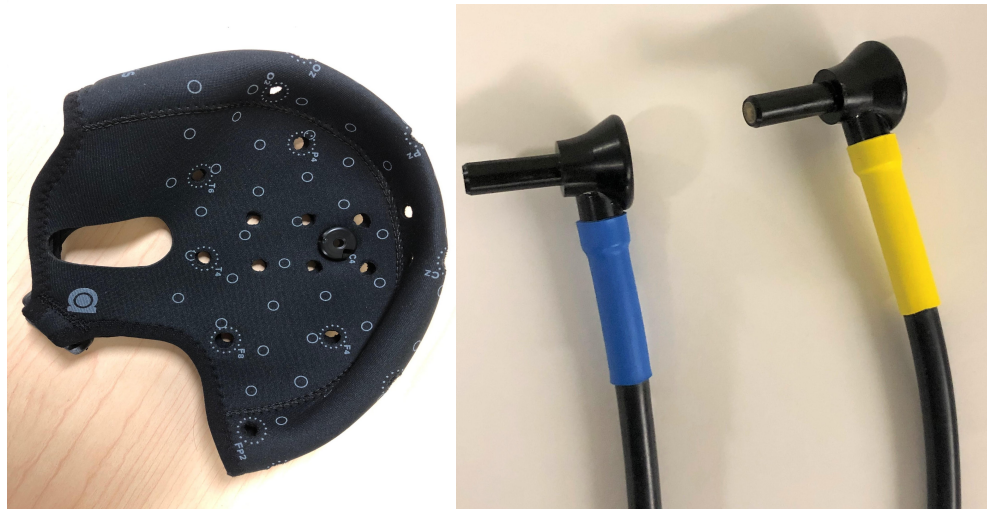


Figure 6: The electroencephalogram headcap used for functional Near-Infrared Spectroscopy data collection and the associated functional Near-Infrared sensors.

The headcap collecting fNIRS data was connected to the OXYMON software as seen in the figure of the Artinis Medical System OXYMON Mk III as displayed below. The data collected using the OXYMON software was converted to a MATLAB data file for analysis. The reflected values for each wavelength are used in conjunction with the Beer-Lambert Law to calculate the oxygenated and deoxygenated hemoglobin concentrations.



Figure 7: The Artinis Medical System used for functional Near-Infrared Spectroscopy data collection.

The blood pressure cuff and plethysmography sensor were connected to the BIOPAC software and were required to be separately recorded. Two lab technicians were required to successfully run the experiment.

5.0. Data Collection

Unfortunately, due to COVID-19 protocols on physical distancing, the data collection process was interrupted, and the experiment was halted before completion. This paper is therefore focused on procedure, set-up, and theoretical analysis of data collected. Going forward, more data collected using this procedure will be essential to drawing strong empirical conclusions about the effect of blood pressure and blood velocity on oxygenation levels. Continuing this research will be critical to determining the accuracy of the theoretical MATLAB model.

The following results are a presentation of the modelled capabilities using acquired test data and cannot be analyzed for trends or definitive relationships. The OXYMON motor imagery and execution fNIRS experimental data was collected in one sitting for each participant.

The data used throughout this report only considers the motor imagery and motor execution trials conducted for two participants as the experiment was halted due to COVID-19 protocols following this data set. The two test datasets were originally intended to confirm the functionality of the software and the theoretical presentation of the collected data. At the time of collection, the BIOPAC Photoplethysmogram and blood pressure cuff sensors were not part of the experimental procedure and were therefore not collected. The static blood pressure values for each participant were simply chosen based on expected values for each participant due to age and fitness. The BIOPAC test data used to generate the results below was derived from a different participant than the initial OXYMON data.

5.1. Data Inaccuracies Resulting from Halted Testing

The initial testing included two motor imagery and motor execution trials with different participants. Additionally, initial Photoplethysmogram and blood pressure data was collected before testing was halted. The collected test-based datasets were inaccurate however, with signal noise present in the second dataset that impacted the quality of analysis. All results for the relevant recorded channels for each participant can be seen in 5.2. Functional Near-Infrared Spectroscopy Data, 5.3. Blood Pressure Data and 5.4. Photoplethysmogram Data.

The BIOPAC data including the blood pressure measurements and Photoplethysmogram data were unable to be fully tested in the experimental setting as they were a later addition to the testing procedure. With their later addition, only test data was acquired with this equipment and was not collected in tandem with the OXYMON data presented in the results.

5.2. Functional Near-Infrared Spectroscopy Data

The functional Near-Infrared Spectroscopy (fNIRS) data collected from the OXYMON system includes the oxygenated and deoxygenated hemoglobin concentrations. These concentrations were determined by the OXYMON system that uses the Beer-Lambert equation and the fNIRS split transmitter wavelengths to calculate each respective concentration. The graphs below include data which has been filtered and manipulated, as described in 7.0. Signal Filtering, Manipulating, and Processing.

The oxygenated and deoxygenated hemoglobin concentrations were determined for each of the 20 collected channels. The oxygenated hemoglobin values are shown in the figure below for each channel, labelled by channel location. The oxygenation and deoxygenation values shift between positive and negative values relative to the initial recorded values.



Figure 8: Participant 1 Motor Imagery Filtered Data Depicting Oxygenated Hemoglobin Concentration.

The respective graph for the deoxygenated hemoglobin concentrations can be seen below. The positive and negative values shown in the oxygenated and deoxygenated graphs represent the recorded hemoglobin characteristics over time and can be used in analysis for blood properties and arterial oxygen saturation.

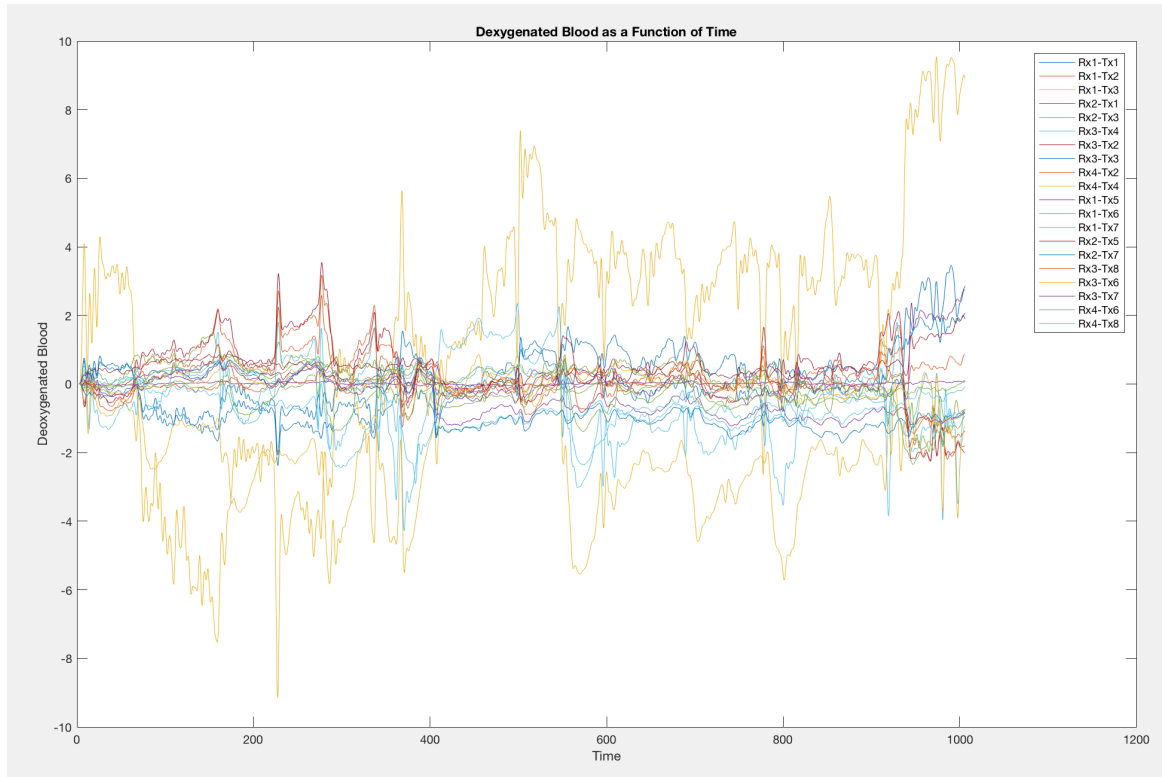


Figure 9: Participant 1 Motor Imagery Filtered Data Depicting Deoxygenated Hemoglobin Concentration.

The fNIRS data was collected from channels placed all over the head to ensure data from varying neural regions. As the different regions of the brain are relevant to specific physical regions of movement, the stimuli-related states of left- and right-hand motions only require analysis for some of the channels recorded. In this data collection process for each hand movement, there were ten channels considered relevant. The data presented throughout this report therefore only considers the relevant channels in analysis and figure presentation. The rest state condition, however, is relevant for all channels as the data pertains to both sides of the body and therefore the rest state data represents all collected channels.

The considered channels with their relevant states and labels are presented in the following table.

Table 3: fNIRS Channel Descriptions.

Channel Number	Channel Label	Relevant States
1	Rx1-Tx1	Rest and Left
2	Rx1-Tx2	Rest and Left
3	Rx1-Tx3	Rest and Left
4	Rx2-Tx1	Rest and Left
5	Rx2-Tx3	Rest and Left
6	Rx3-Tx4	Rest and Left

7	Rx3-Tx2	Rest and Left
8	Rx3-Tx3	Rest and Left
9	Rx4-Tx2	Rest and Left
10	Rx4-Tx4	Rest and Left
11	Rx1-Tx5	Rest and Right
12	Rx1-Tx6	Rest and Right
13	Rx1-Tx7	Rest and Right
14	Rx2-Tx5	Rest and Right
15	Rx2-Tx7	Rest and Right
16	Rx3-Tx8	Rest and Right
17	Rx3-Tx6	Rest and Right
18	Rx3-Tx7	Rest and Right
19	Rx4-Tx6	Rest and Right
20	Rx4-Tx8	Rest and Right

5.3. Blood Pressure Data

The blood pressure of each tested individual is measured using a blood pressure cuff placed on the participant's bicep with the data recorded through the BIOPAC system. The blood pressure readings captured can be used to calculate an average blood pressure value, either throughout the entire trial or at initial calibration period, to determine a static blood pressure value for the participant [26]. This static blood pressure value can be used as a metric for determining a participant's blood pressure condition and classification as normal or hypertensive blood pressure, which is useful for analysis. The entirety of the blood pressure dataset can be used for continuous blood pressure analysis with identified trends comparable against other gathered recordings. The recorded continuous blood pressure test data is presented in the figure below.

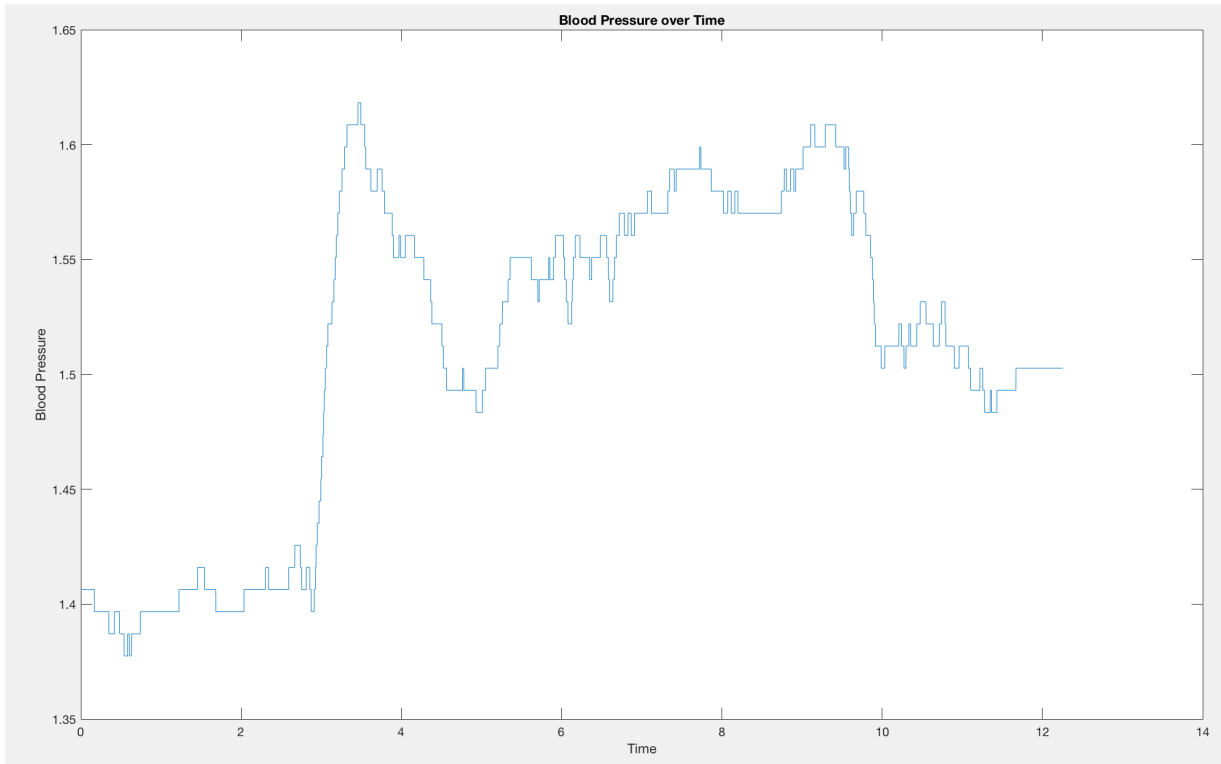


Figure 10: Blood Pressure Testing Data.

5.4. Photoplethysmogram Data

The Photoplethysmogram device was attached on the tip of the participant's index finger and the corresponding data was recorded using the BIOPAC system. The PPG signal shows the variance in the infrared signal received over time, which can be used to calculate blood volume, blood pressure, oxygen saturation, heart rate, and the point of heart systole [27] [28]. The raw signal recorded by the BIOPAC system, as shown in the figure below, provides enough information to calculate the metrics in the developed code.

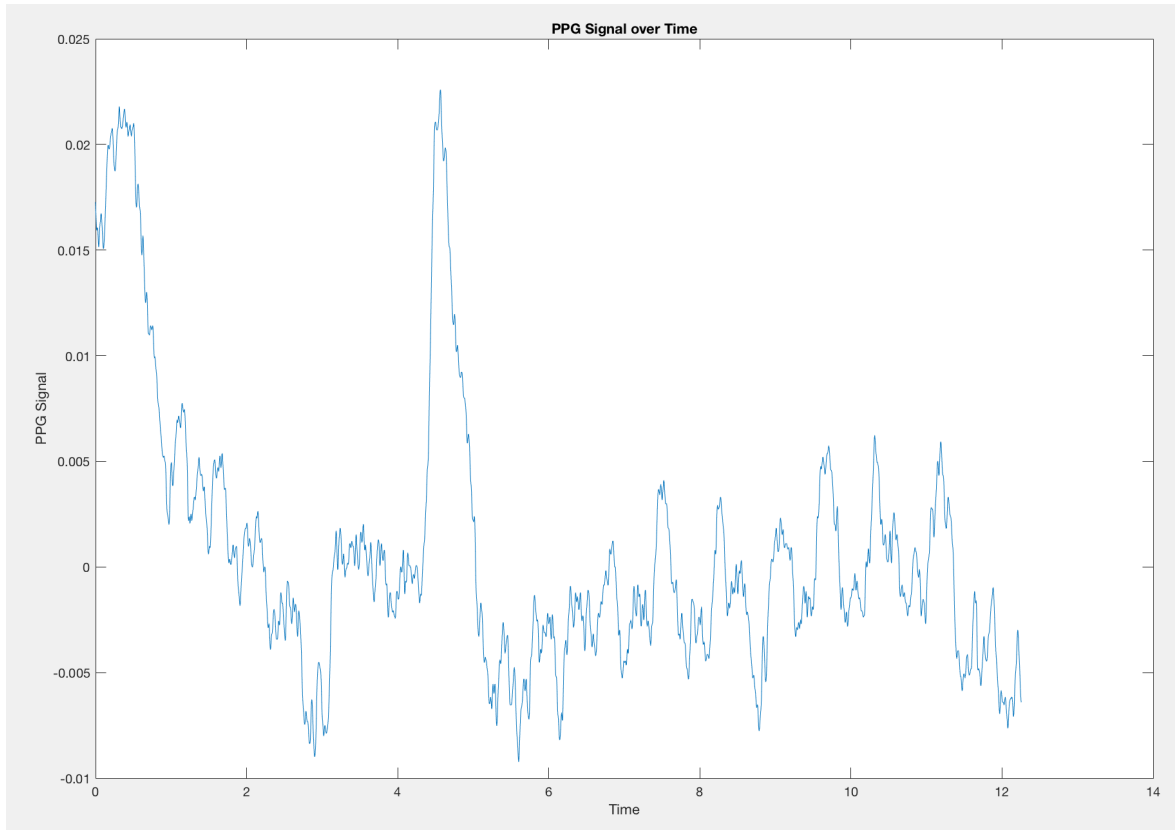


Figure 11: Photoplethysmogram Testing Data.

6.0. Developed Empirical Analysis Software

With the collected test data, a flexible software repository was developed using MATLAB to interpret and analyze the collected data. Although the software was only tested using the limited data samples, it was designed to be flexible and modular so that the software will be successful with varying amounts of data and data structures.

6.1. Software Structure and Capabilities

The developed software was designed with a singular main script which the technician would run as to limit confusion. The majority of the computation and display functionalities offered with this software are available through different functions in the repository which can be called upon by the main script.

The software was developed with the intention of providing a useable MATLAB library that analyzes fNIRS, PPG, and blood pressure data. The developed MATLAB features datasets as individual and combined measurements. The software aims to be simple, flexible, and easily learned with few global variables that can be edited to adjust parameters throughout the code. An example of this modularity is the channel variables, which defines the total number of channels as well as the relevant channels for each stimulus in the procedure. By changing each of these three channels, the channel variables change throughout the code. This flexibility allows the conducted experiment to involve varying numbers of fNIRS channels and only requires changing one variable for each considered stimulus.

The developed functions pertain to the following processing, calculations, and analysis:

- PPG and Blood Pressure Signal Processing;
- PPG Calculations for Peaks, Heart Rate, and Derivatives;
- fNIRS Filtering and Signal Processing;
- Display and Analysis of individual test results;
- State Comparison across Motor Imagery and Motor Execution;
- Action Comparison around Right/Left/Rest Stimuli Events;
- Participant Comparison for MI/ME Analyzing Blood Pressure and Oxygenation Percentage; and
- Comparison of Continuous Blood Pressure and Oxygenation Percentage.

Each stimulus time was recorded by the visual presentation software and was recorded in the OXYMON software as an event. Each event corresponded to an array of sample values for each stimulus that identified the start sample for the stimulus. This was used in analysis to separately consider the physiological result of each stimulus, including both right and left arrows as well as rest times. The times considered were globally defined variables similar to channel numbers for each stimulus to allow for changes in the time considered after each stimulus.

6.2. Analysis Potential

Both the measured and calculated metrics were organized for potential analysis through the graphical representation of averaged metrics with potential relationships considered for trends. Each calculation and potential trend is outlined in Section 8.0: Expected Analysis. The produced trends should be carefully qualitatively and quantitatively analyzed for relationships between the motor imagery and execution experiments, the stimulus events, the measured blood volume, and the participant's recorded static and continuous blood pressure.

7.0. Signal Filtering, Manipulating, and Processing

The raw fNIRS data was first manipulated to remove large signal errors such as incorrectly calibrated channels or channels with poor connection to limit errors. For each channel deemed inaccurate, the software would correct the data and produce a message highlighting the error to the technician. The technician could choose to remove the channel in its entirety or to ignore the channel data in analysis. Additionally, the fNIRS data was filtered to decrease the signal noise present in the measurements to allow for cleaner and more accurate data in analysis. The details of the manipulation and filtering processes are outlined in Section 7.1.

7.1. Manual Functional Near-Infrared Spectroscopy Data Manipulations

The data from participant 2 for all 20 channels of motor imagery data can be seen below. Throughout the 1000 second trial, the oxygenated and deoxygenated blood levels for each channel had a visible issue with one of the channels. Channel 1 (labelled as Rx1-Tx1) has an averaged oxygenated hemoglobin concentration of approximately -8. This divergence from the expected median of approximately 0 can be assumed to be a hardware or equipment connection malfunction and should not be considered as accurate signal values. The motor execution data for participant 2 additionally had significant signal connection issues towards the end of the trial - data reached unreasonable oxygenation and deoxygenation ranges. These connection issues are visible in the below graph towards the end of the trial with the oxygenation values diverging towards infinity. The raw oxygenated hemoglobin concentration data without manipulation for all 20 channels collected from test dataset 2 can be seen in Figure 12.

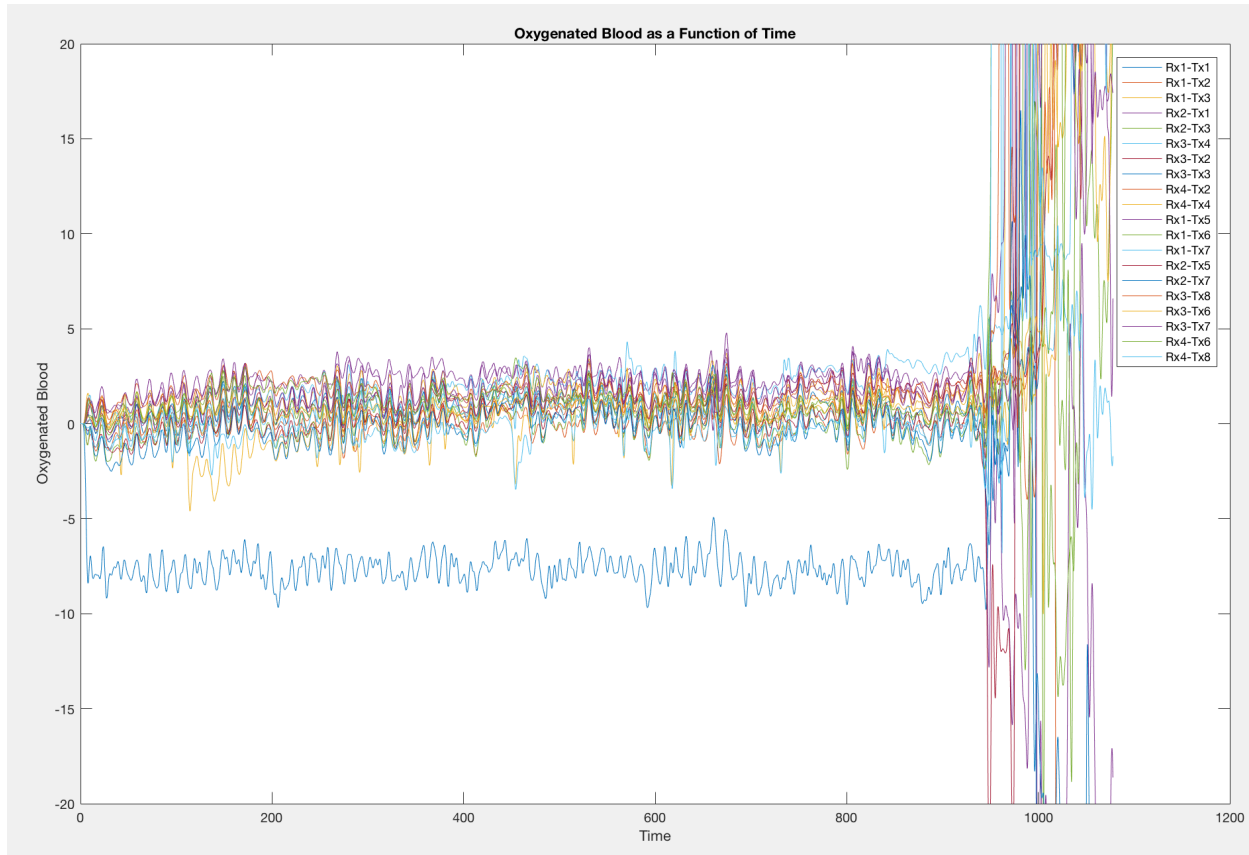


Figure 12: Participant 2 Motor Imagery Filtered and Unmanipulated Data Depicting Oxygenated Hemoglobin Concentration.

To use this test data in the developed software, manual adjustments were made by removing infinite data from signal connection issues. The infinite signal connections were mitigated manually in the code by limiting the maximum oxygenation and deoxygenation levels to the range of [-10,10]. The value of 10 was chosen as it is high enough above expected values to not be considered accurate data while remaining in an acceptable range to view the remaining data. The data was then manipulated by moving the averaged value of the outlying data channel to be centered around 0. This adjustment allows the incorrect data to be compared to the accurate data for theoretical analysis conducted with the test data. This manual adjustment was conducted for both the motor imagery and motor execution data for participant 2. The updated values are presented in Figure 13 below. For this particular dataset of participant 2 under the motor imagery trials, all channels have had their data range set to [-10, 10] and channel 1 has been moved to centre around a concentration of 0.

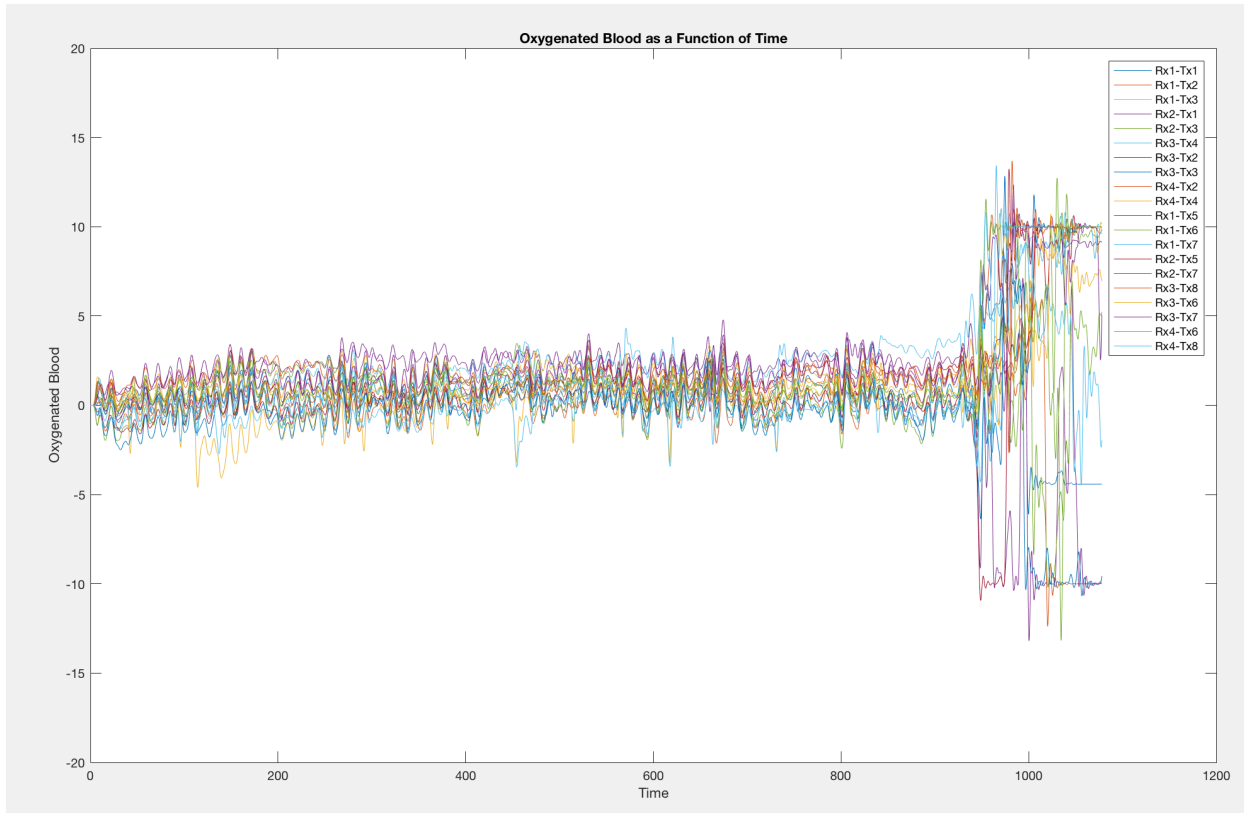


Figure 13: Participant 2 Motor Imagery Filtered and Manipulated Data Depicting Oxygenated Hemoglobin Concentration.

The data had to be limited to a range from [-10 10] before moving the data to be centered around 0 as without this edit the diverging data affected the channel's mean values. This resulted in some channels initially centered around 0 being readjusted to inaccurately be centered around non-zero values, as seen with the new displacement of Channels Rx3-Tx8, Rx3-Tx6, and Rx4-Tx6 below.

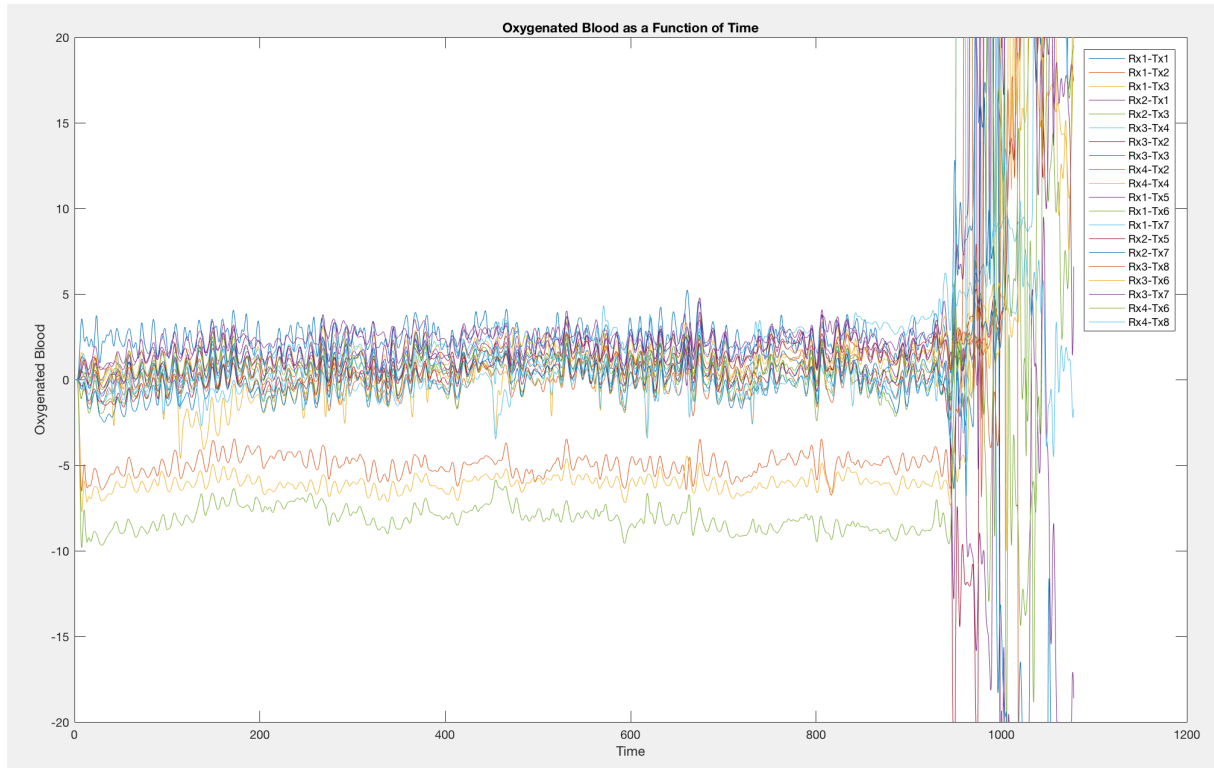


Figure 14: Participant 2 Motor Imagery Filtered Data Depicting Oxygenated Hemoglobin Concentration Only edited for Corruption.

Finally, there were software issues in the conversion of the OXYMON fNIRS data to the MATLAB data structure that impacted the collected data. In the data structure conversion process, some of the collected samples were removed which resulted in the experimental data not describing the entire experimental process. This affected the software such that the stimulus onset values, which record the presentation of each stimulus separately as a sample number, in some cases exceeded the number of samples kept in the MATLAB data structure. To overcome this issue, the onset values that exceeded the data sample size were set to be the final sample value and therefore discarded. The number of trials conducted for each edited stimulus were updated accordingly to reflect the accurate number of trials presented in the data.

7.2. Functional Near-Infrared Spectroscopy Data Filtering

The formal data processing included a lowpass butterworth filter with a cutoff frequency of 0.2 Hz, as used in fNIRS signal processing reviews [29] [30]. This filter produced significantly cleaner data for analysis. The following graph displays all channels of the filtered and unfiltered data for the motor imagery trials conducted for participant 1.

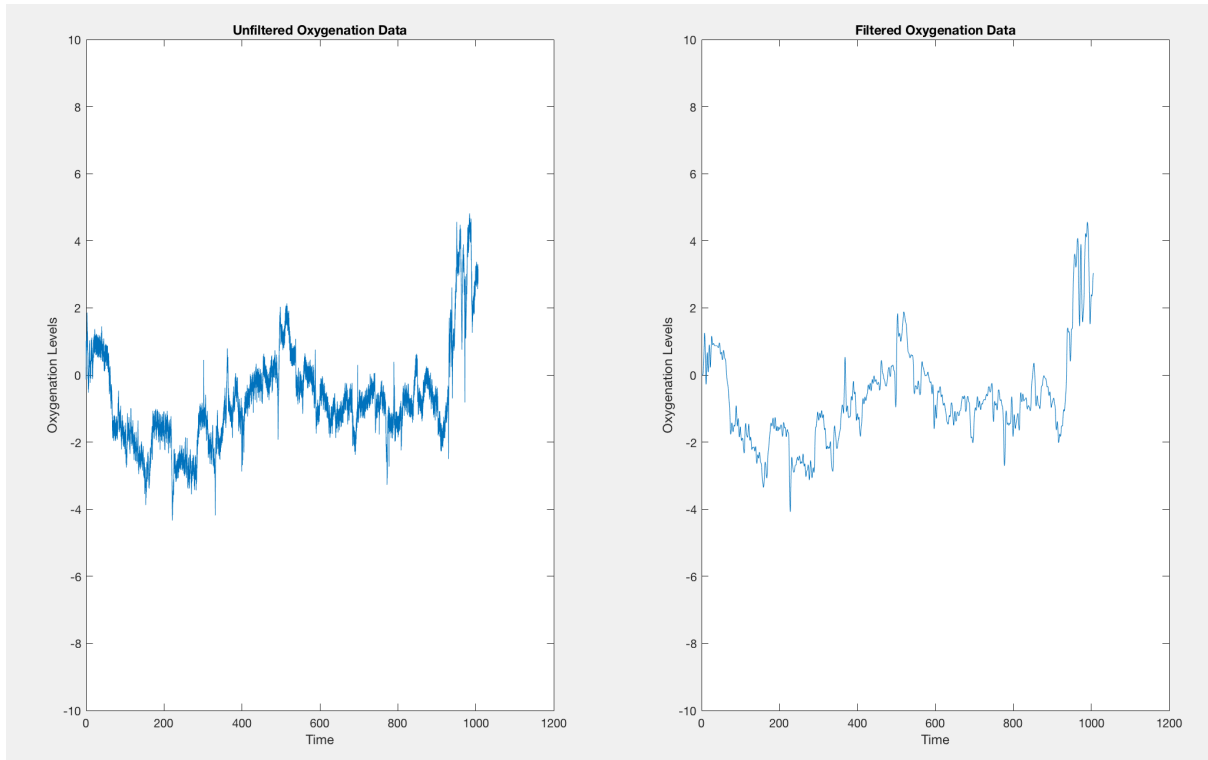


Figure 15: Participant 2 Motor Imagery Filtered and Unfiltered Data Depicting Oxygenated Hemoglobin Concentration.

7.3. Photoplethysmogram Data Filtering

The Photoplethysmogram (PPG) device was attached to the tip of the left index finger and the measurements were collected using the BIOPAC software system. The raw test data was produced on a singular channel and was filtered using a butterworth notch filter between 59 and 61 Hz to remove the 60 Hz noise caused by the powerlines.

8.0. Applied Calculations

8.1. Photoplethysmography Calculations

The Photoplethysmography (PPG) data, filtered and with each determined systolic peak point labelled with a vertical red dotted line, can be seen in the figure below. The systolic peak values can be used to approximate fluctuations in blood velocity as these peaks occur at the point of maximum positive pressure. These identified peaks could be used in future trend analysis to calculate heart metrics such as heart rate variability [34].

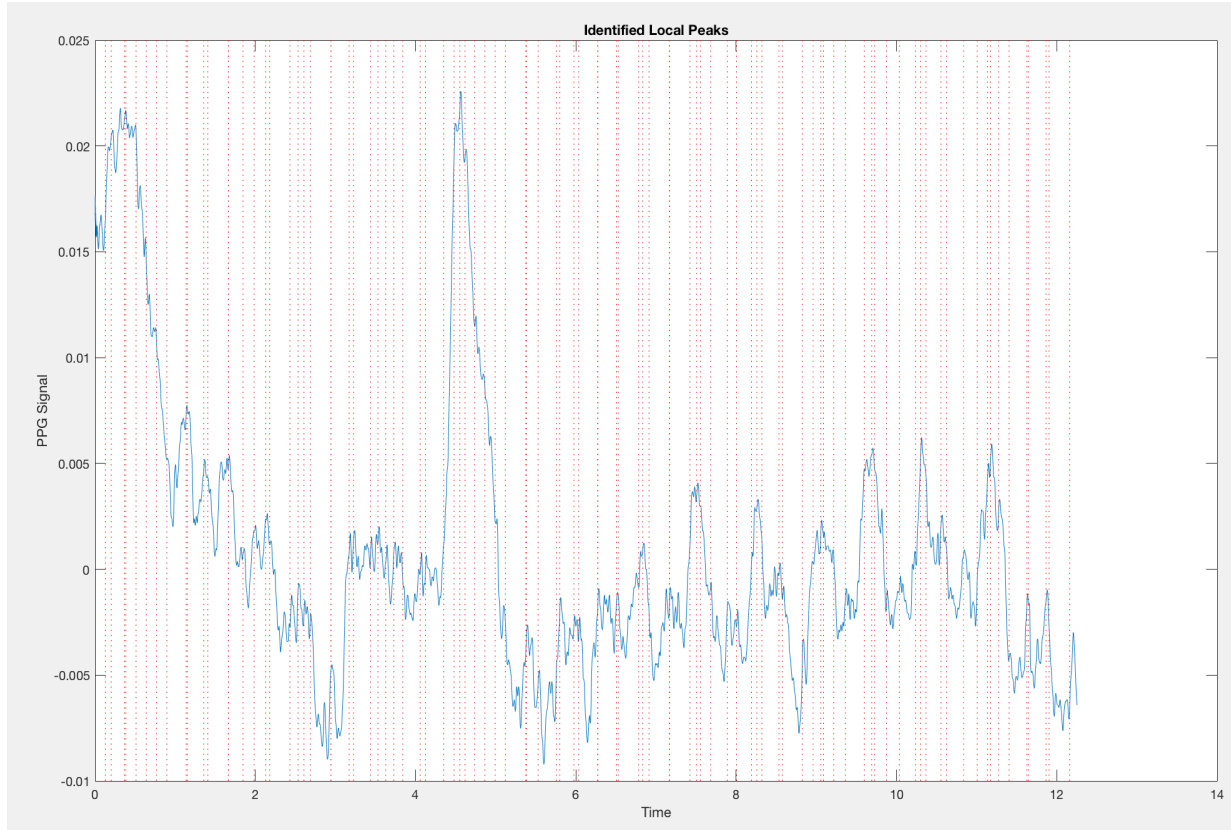


Figure 16: Photoplethysmogram Data Including Identified Peaks.

Common metrics used in PPG data analysis are the PPG derivatives. The second derivative of the PPG data, as shown in the figure below, is the Acceleration Photoplethysmogram (APG) and is an indicator of the acceleration of blood [31]. The derived APG is often used to detect and diagnose cardiac abnormalities and other health conditions such as the arterial stiffness index and an ageing index [32]. Providing the derivative calculation as a feature in the software package allows for further trend analysis between the arterial stiffness index, ageing index, and fluid dynamic blood and blood vessel properties.

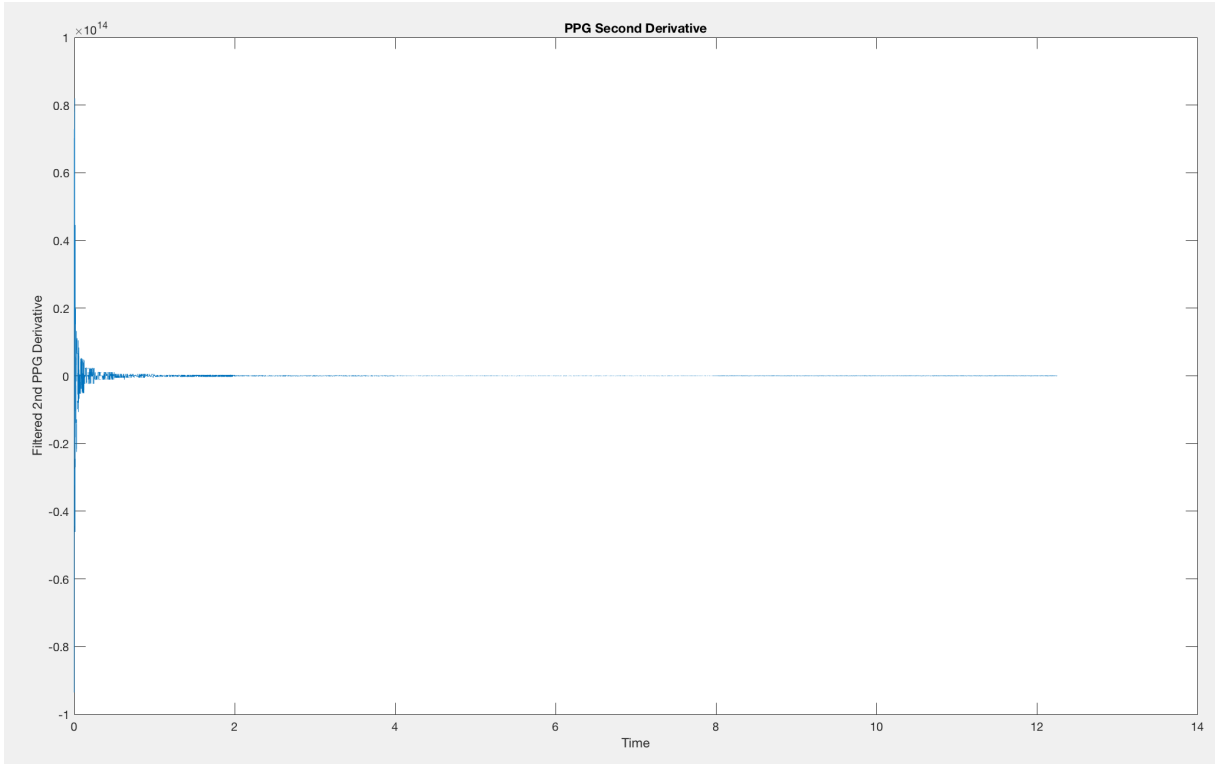


Figure 17: Photoplethysmogram Data Derived Twice.

In the derivative analysis, the metrics produced can be used to consider the blood pressure and fNIRS data in terms of the heart rate and systolic peak as arterial system properties.

8.2. Blood Pressure Calculations

The measured data from the blood pressure cuff was used to define a static blood pressure value that can be used as a metric in analysis. The average blood pressure value was determined using a set calibration time with the participant sitting still for the duration of the calibration.

8.3. Functional Near-Infrared Spectroscopy Calculations

The main calculations resulting from the oxygenated and deoxygenated hemoglobin values are the blood volume and oxygenated percentage values. The blood volume is the sum of the oxygenated and deoxygenated hemoglobin, as the amount of hemoglobin movement can be considered as the total amount of blood. As the fNIRS data is respective to the initial value, all data values are considered in terms of the initial state so both positive and negative values are expected and logical. The data for the oxygenated and deoxygenated hemoglobin concentration as well as the result of their associated blood volume concentrations can be seen below for participant 1's MI trials.

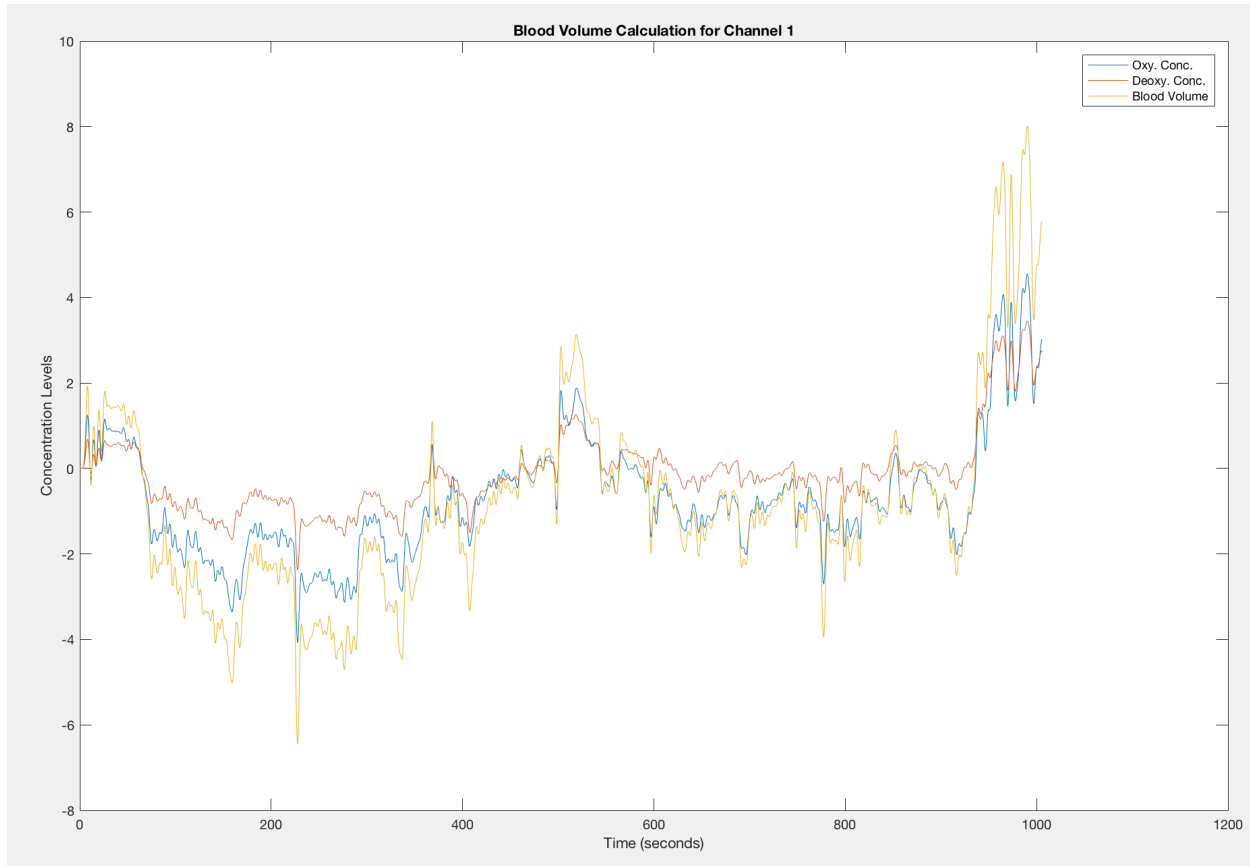


Figure 18: Participant 1 Motor Imagery Filtered and Manipulated Data Depicting Oxygenated Hemoglobin Concentration and Deoxygenated Hemoglobin Concentration and Blood Volume for Channel 1.

The percentage of oxygenated hemoglobin was calculated by considering the changing concentration of oxygenated hemoglobin as a factor of the total changing blood volume. As the fNIRS measurement technique only considers the change in concentration levels using the initial state as a baseline, there are contexts which have a non-zero value in the concentration of oxygenated hemoglobin but a zero value in the blood volume due to the change in the concentration of deoxygenated hemoglobin. This scenario results in oxygenated percentage data that is difficult to qualitatively or quantitative analyze. An example of the diverging infinite data can be seen in the figure below.

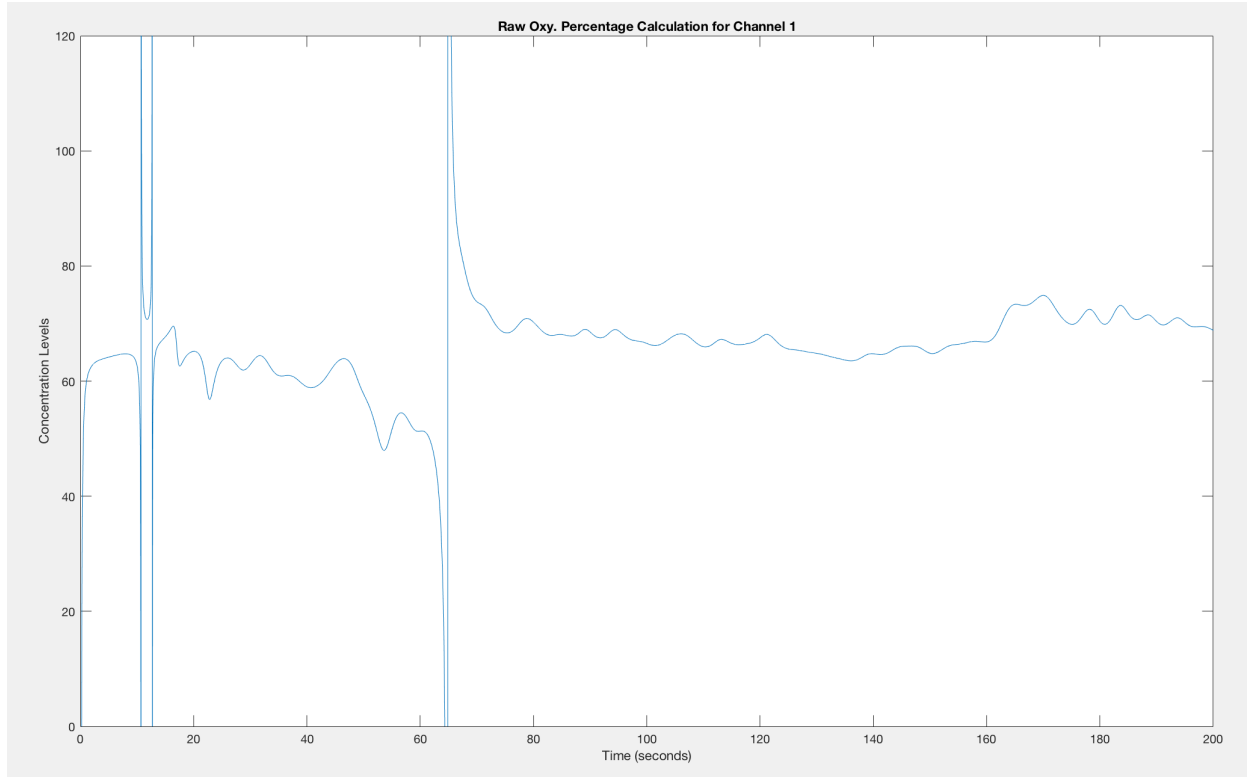


Figure 19: Participant 1 Motor Imagery Filtered and Manipulated Data Depicting the Percentage of Oxygenated Hemoglobin Concentration for Channel 1.

To overcome these data errors a moving average filter was developed to identify unreasonably large spikes and remove them from the data. To accomplish this, the data was separated into epochs that could be separately analyzed and edited. Within each epoch, the mean value of the epoch and the difference between the minimum and maximum recorded values were calculated. If the difference between the maximum and minimum oxygen percentage values recorded in the epoch were above a set threshold of 30, the values were instead set to NaN values and were removed from the data. Although this method did not completely clean the data, this method significantly improved the remaining data so that it could be used for analysis.

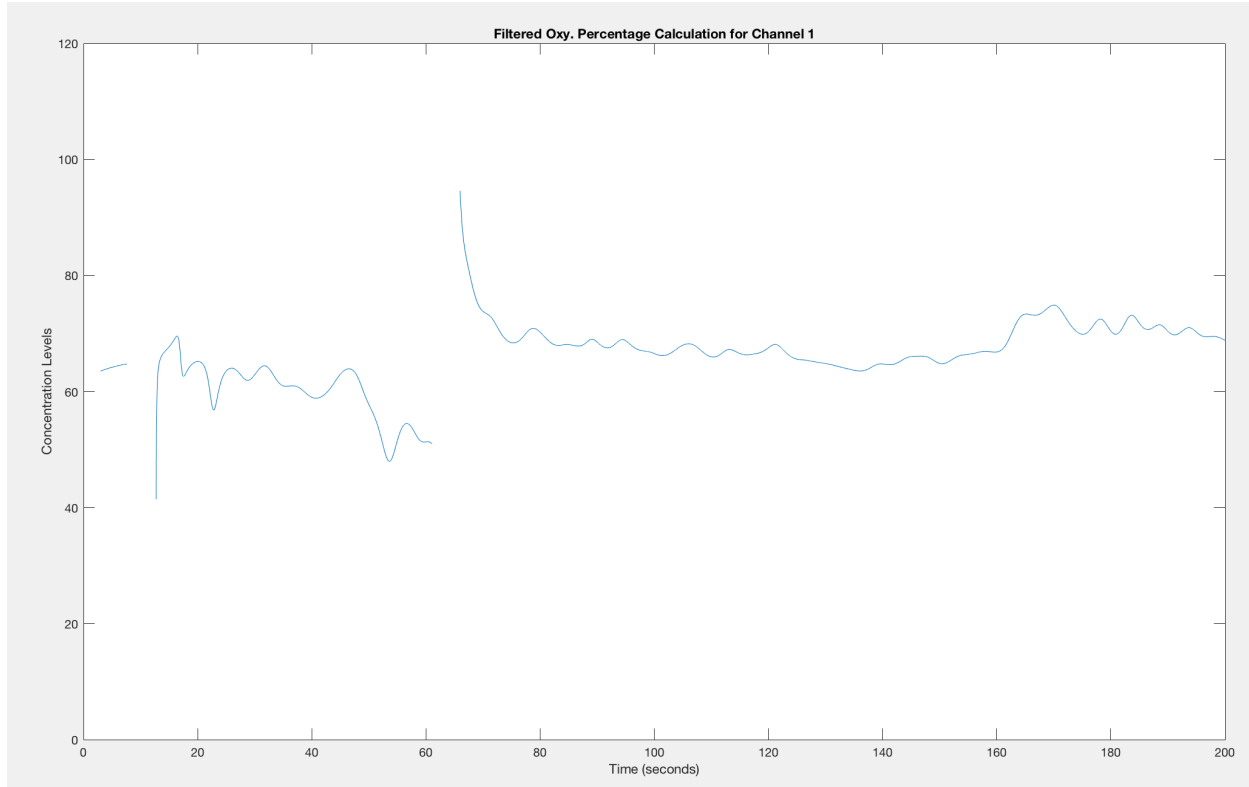


Figure 20: Participant 1 Motor Imagery Filtered and Manipulated Data Depicting the Percentage of Oxygenated Hemoglobin Concentration for Channel 1 with the Applied Moving Average Filter Edits.

8.4. Functional Near-Infrared Spectroscopy Averaged Values

To accurately consider the trends associated with the fNIRS data, the data of each participant was segmented into the three stimuli, rest, and right or left for each of the two trials for motor imagery and motor execution. The analysis time chosen for each presented stimulus was 10 seconds following the stimulus presentation. For each separate segment, the 10 second dataset was averaged. The averaged values were calculated for the oxygenated hemoglobin concentration, the deoxygenated hemoglobin concentration, the measured blood volume, and the measured oxygen percentage. These trends could be analyzed across numerous participants and trials to identify relationships.

The following figure shows the average calculated blood volume for participant 1's motor imagery experiments in the 10 seconds following each stimulus. The relevant channels for the three stimuli are presented side-by-side for qualitative comparative trend analysis.

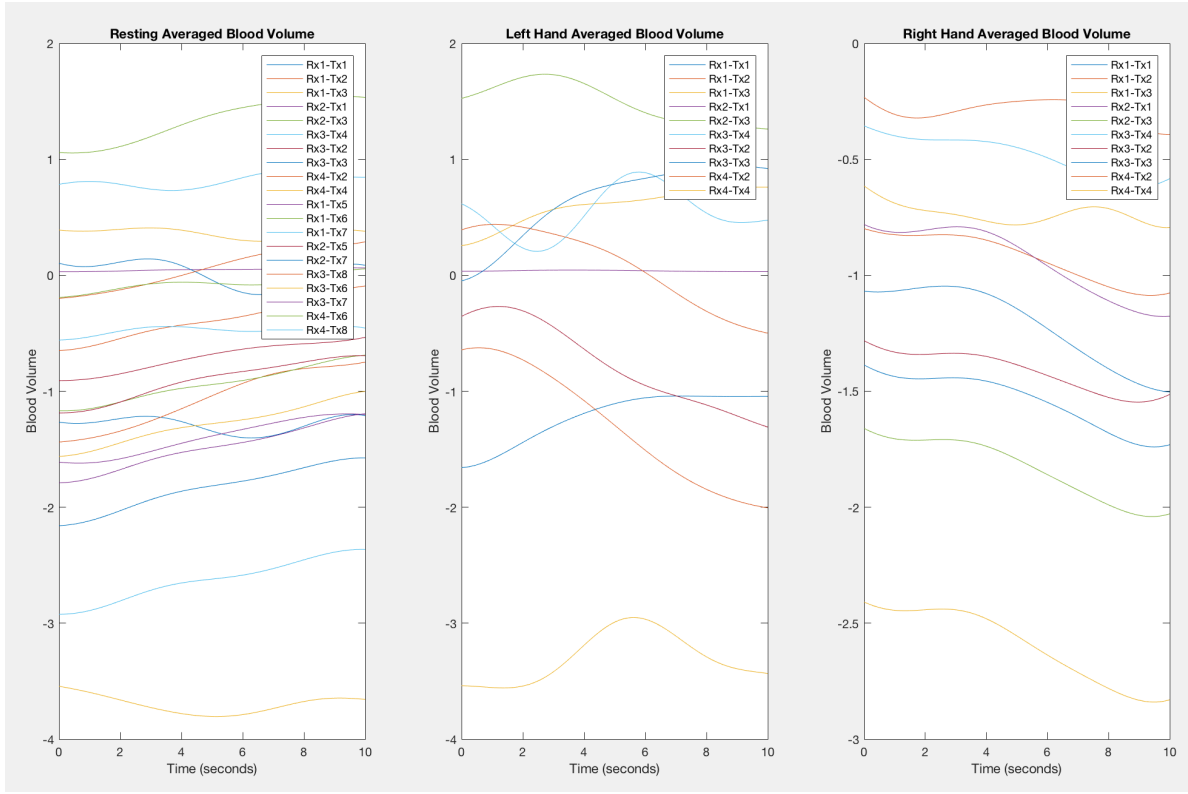


Figure 21: Participant 1 Motor Imagery Filtered and Manipulated Data Depicting the Averaged Epoch for Blood Volume for the Relevant Channels of each State: Rest, Right, and Left.

The following figure shows the average calculated oxygen percentage for participant 1's motor imagery experiments in the 10 seconds following each stimulus. The relevant channels for the three stimuli are presented side-by-side for qualitative comparative trend analysis.

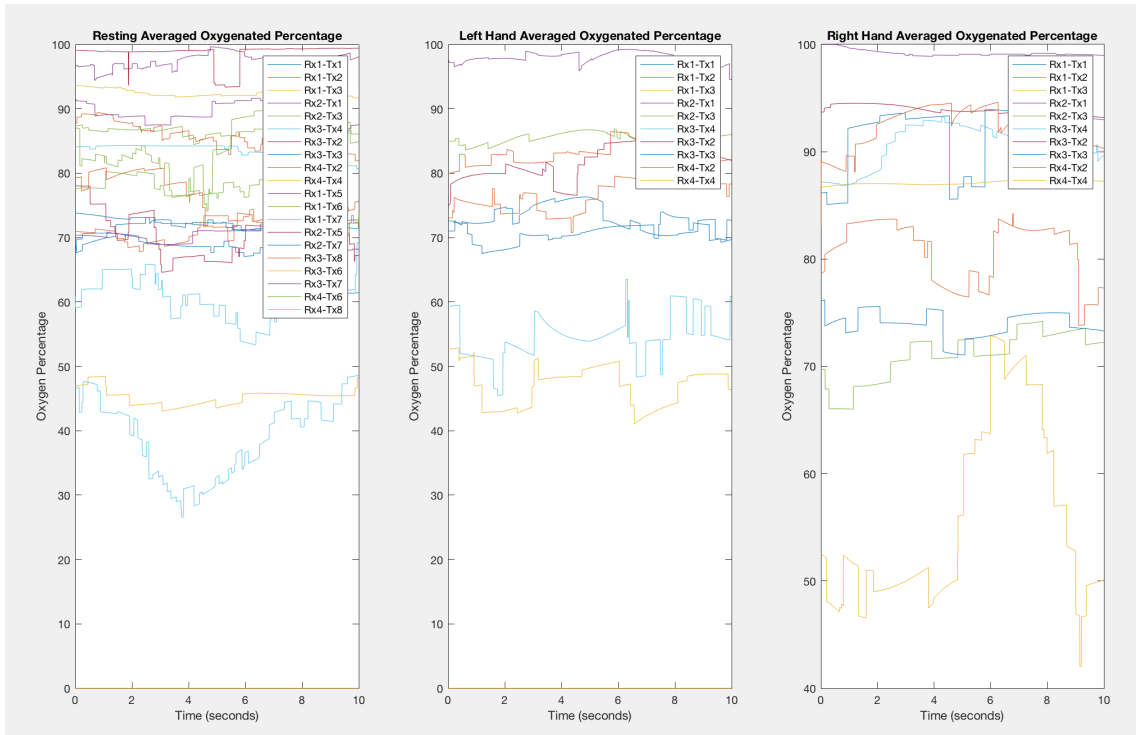


Figure 22: Participant 1 Motor Imagery Filtered and Manipulated Data Depicting the Averaged Epoch for the Percentage of the Oxygenated Hemoglobin Concentration for the Relevant Channels of each State: Rest, Right, and Left.

Additional graphs displaying the fNIRS averaged values for the oxygenated and deoxygenated hemoglobin concentrations can be seen in Appendix B: Additional Graphs.

9.0. Expected Analysis

Through the collected data and the developed software, the following graphs were produced to identify trends between the motor imagery and execution experiments, the stimulus events, the measured blood volume, and the participant's recorded static and continuous blood pressure. If another technician was to collect this data, it would be imperative for them to carefully qualitatively and quantitatively consider each produced figure for relationships. To consider each potential relationship, functions were developed to analyze and display each potential trend individually.

9.1. State Comparison Analysis

The three considered states for both the motor imagery and motor execution trials were the left state, the stimulus-initiated right movement, and the stimulus-initiated left movement. Each considered state was described by 10 second epochs which were averaged for the following analysis. For each considered stimulus, the values for oxygenated hemoglobin concentration, deoxygenated hemoglobin concentration, blood volume, and oxygen percentage were considered. The right and left state averaged epochs were considered in terms of the rest state averaged epoch for potential trends. These states were determined for each variable by subtracting each movement state epoch from the rest state epoch.

The following figure shows the oxygenated hemoglobin concentration averaged epoch differences for each of the right and left states in terms of the rest state for participant 1 in the motor imagery experiment.

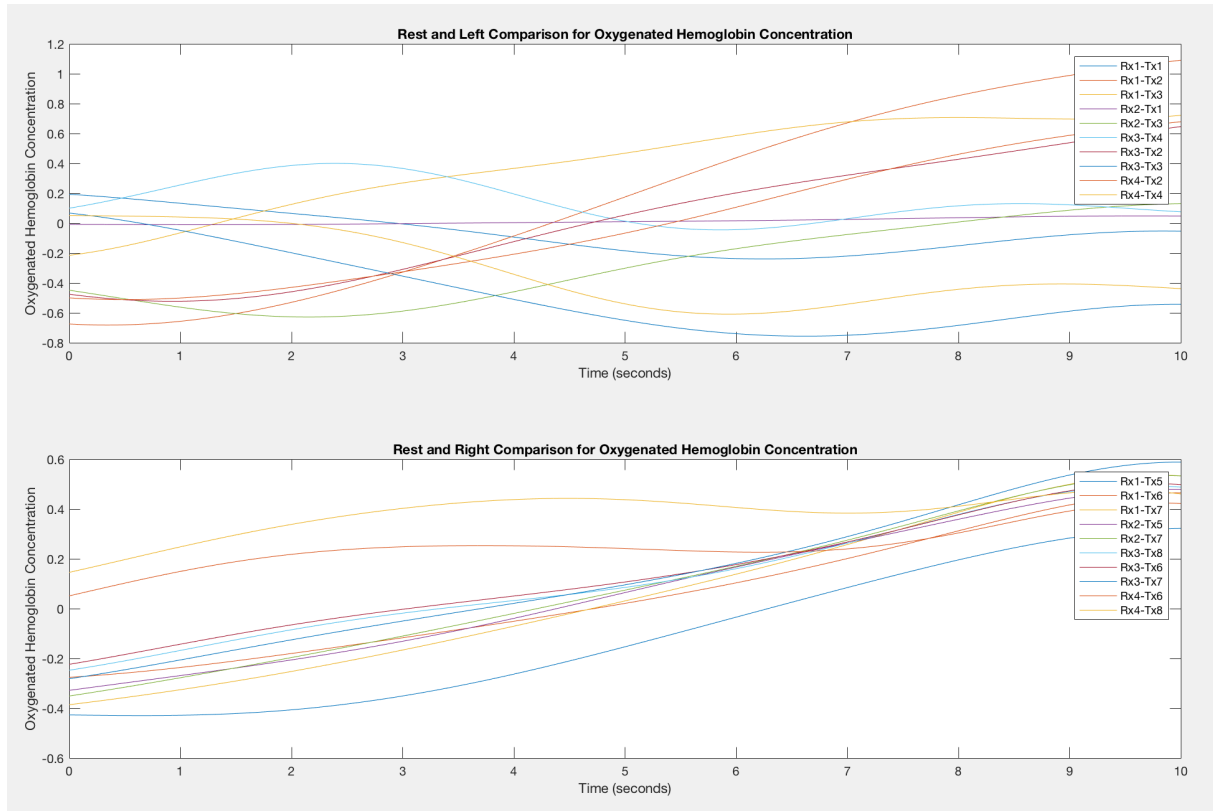


Figure 23: Participant 1 Motor Imagery Filtered and Manipulated Data Depicting the Averaged Epoch Oxygenated Hemoglobin Concentration for the Relevant Channels of the Right and Left States as a Function of the Rest State.

The following figure shows the deoxygenated hemoglobin concentration averaged epoch differences for each of the right and left states in terms of the rest state for participant 1 in the motor imagery experiment.

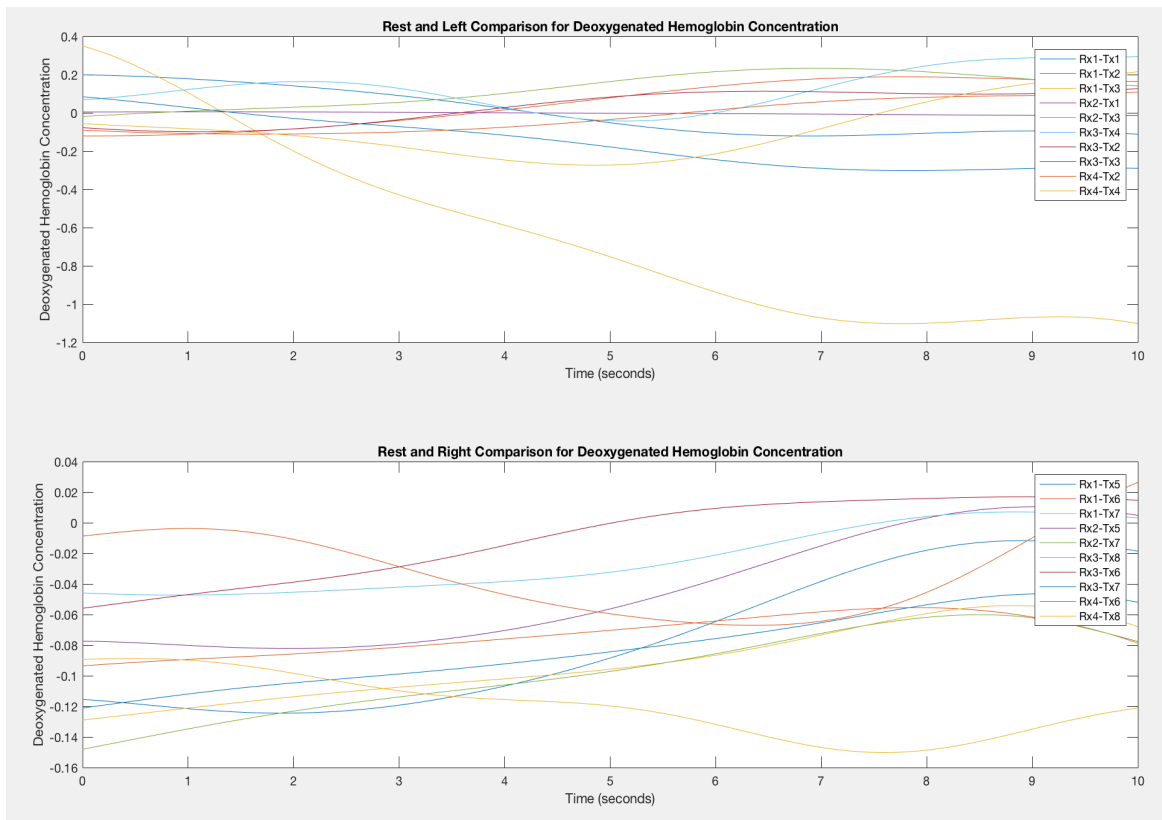


Figure 24: Participant 1 Motor Imagery Filtered and Manipulated Data Depicting the Averaged Epoch Deoxygenated Hemoglobin Concentration for the Relevant Channels of the Right and Left States as a Function of the Rest State.

The following figure shows the blood volume averaged epoch differences for each of the right and left states in terms of the rest state for participant 1 in the motor imagery experiment.

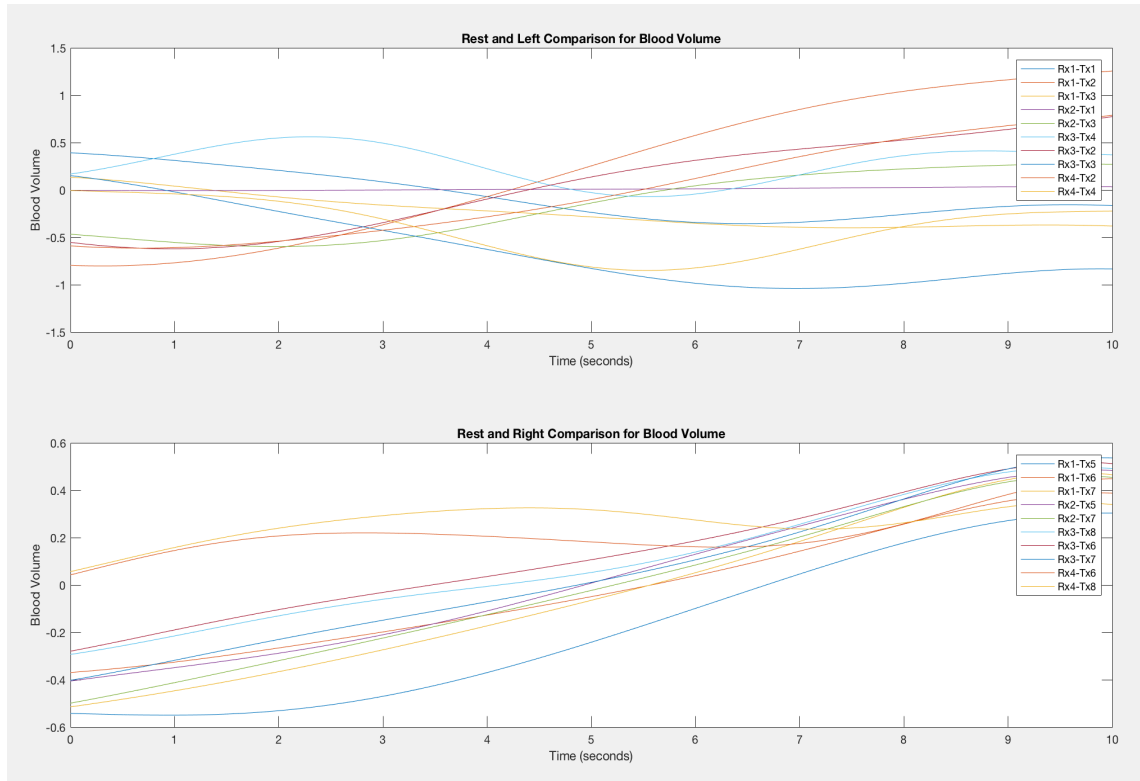


Figure 25: Participant 1 Motor Imagery Filtered and Manipulated Data Depicting the Averaged Epoch Blood Volume for the Relevant Channels of the Right and Left States as a Function of the Rest State.

The following figure shows the percentage of oxygenated hemoglobin averaged epoch differences for each of the right and left states in terms of the rest state for participant 1 in the motor imagery experiment.

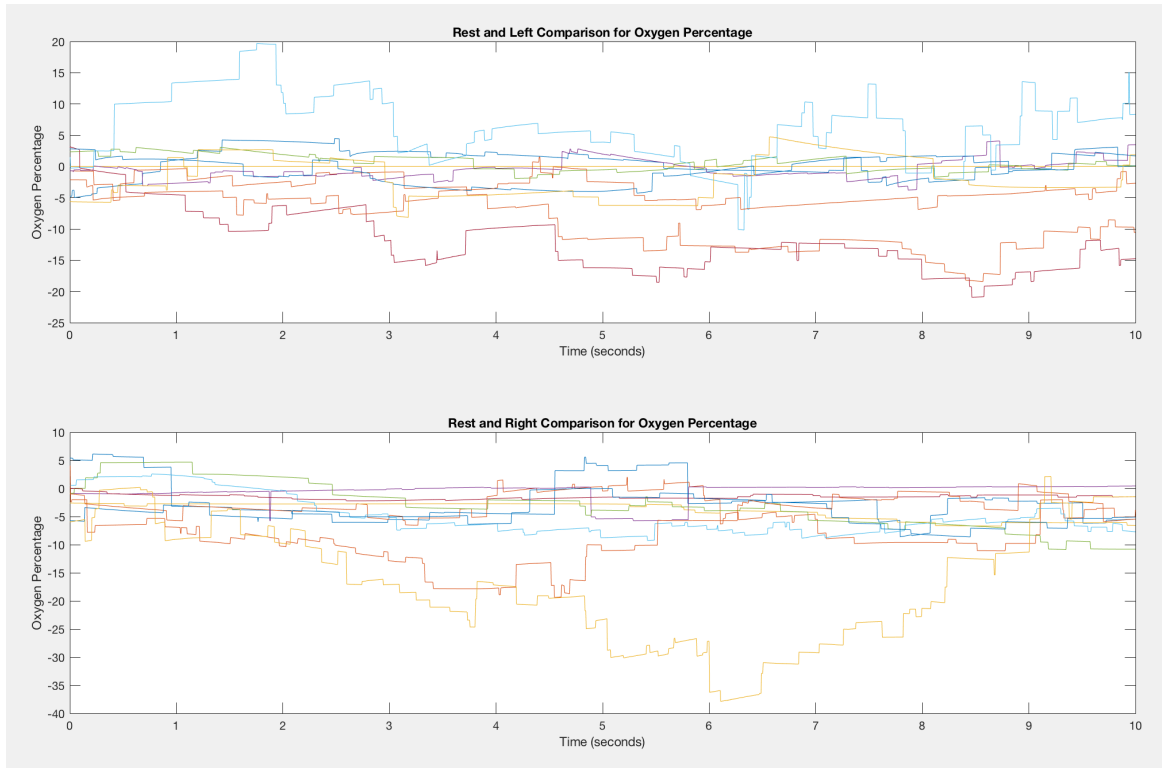


Figure 26: Participant 1 Motor Imagery Filtered and Manipulated Data Depicting the Averaged Epoch for the Percentage of Oxygenated Hemoglobin Concentration for the Relevant Channels of the Right and Left States as a Function of the Rest State.

9.2. Action Comparison Analysis

The motor imagery and motor execution experiments were compared for each variable using the averaged epochs for each resting, right-hand, and left-hand stimulus states. The two experimental trials were compared for each participant dataset by subtracting the motor imagery data from the motor execution data for each considered state. The resulting data, shown in the figure below, was presented for each stimulus and can be considered for potential relationships. The resulting different trial data should be analyzed for average differences for each channel as well as for trends present in each channel which may signify a change in blood flow or oxygen percentage which only appears in one trial.

The following figure shows the blood volume for each of the right, left and rest states as a function of the difference between the motor imagery and motor execution for participant 1's averaged epoch data.

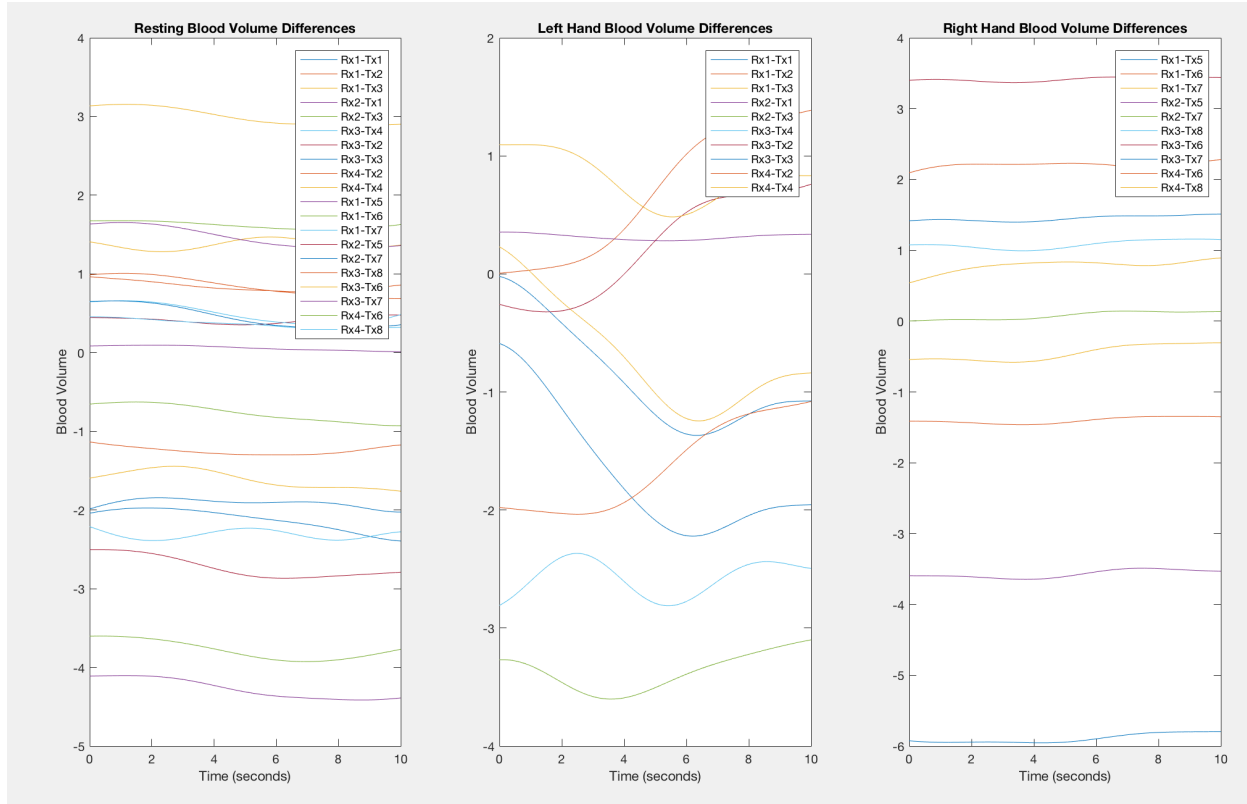


Figure 27: Participant 1 Filtered and Manipulated Averaged Blood Volume Epoch for the Relevant Channels of the Differences between the Motor Imagery and Motor Execution Data for Each State.

The following figure shows the percentage of oxygenated hemoglobin for each of the right, left and rest states as a function of the difference between the motor imagery and motor execution for participant 1's averaged epoch data.

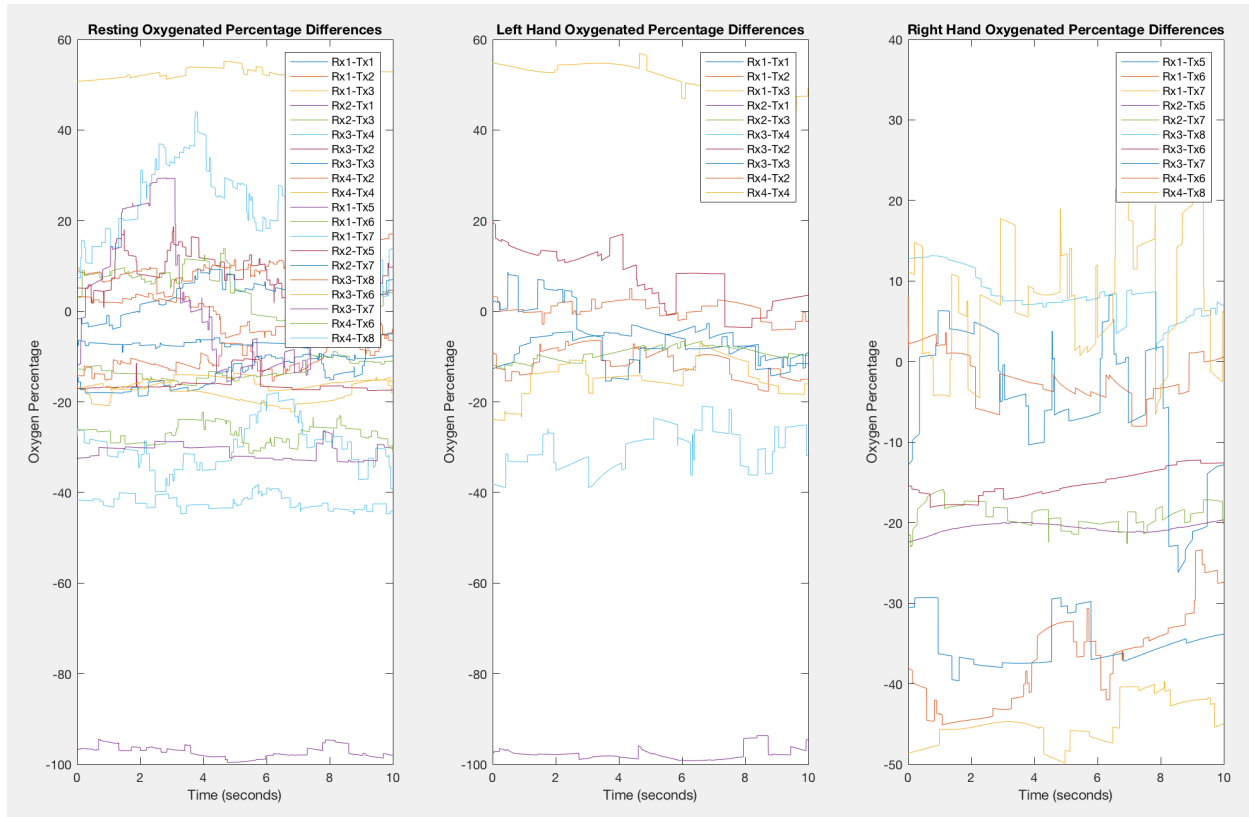


Figure 28: Participant 1 Filtered and Manipulated Averaged Percentage of Oxygenated Hemoglobin Concentration Epoch for the Relevant Channels of the Differences between the Motor Imagery and Motor Execution Data for Each State.

9.3. Participant Comparison Analysis

Two participant datasets were directly compared for each state individually. The differences were calculated for this analysis by subtracting the second considered dataset from the first. This function was developed with significant flexibility so that it could be used for larger-scale analysis than the comparison of two participants as in this analysis. The main purpose of this function with larger collections of data sets would be to directly compare the averaged states of participants with normal and hypertensive conditions across all relevant movement states for each variable while considering each trial separately. Analyzing each variable individually allows for trends and potential relationships to be qualitatively identified clearly with limited confounding factors.

The following figure shows the motor imagery blood volume averaged epoch data for each of the right, left and rest states as a function of the difference between participant 1 and participant 2.

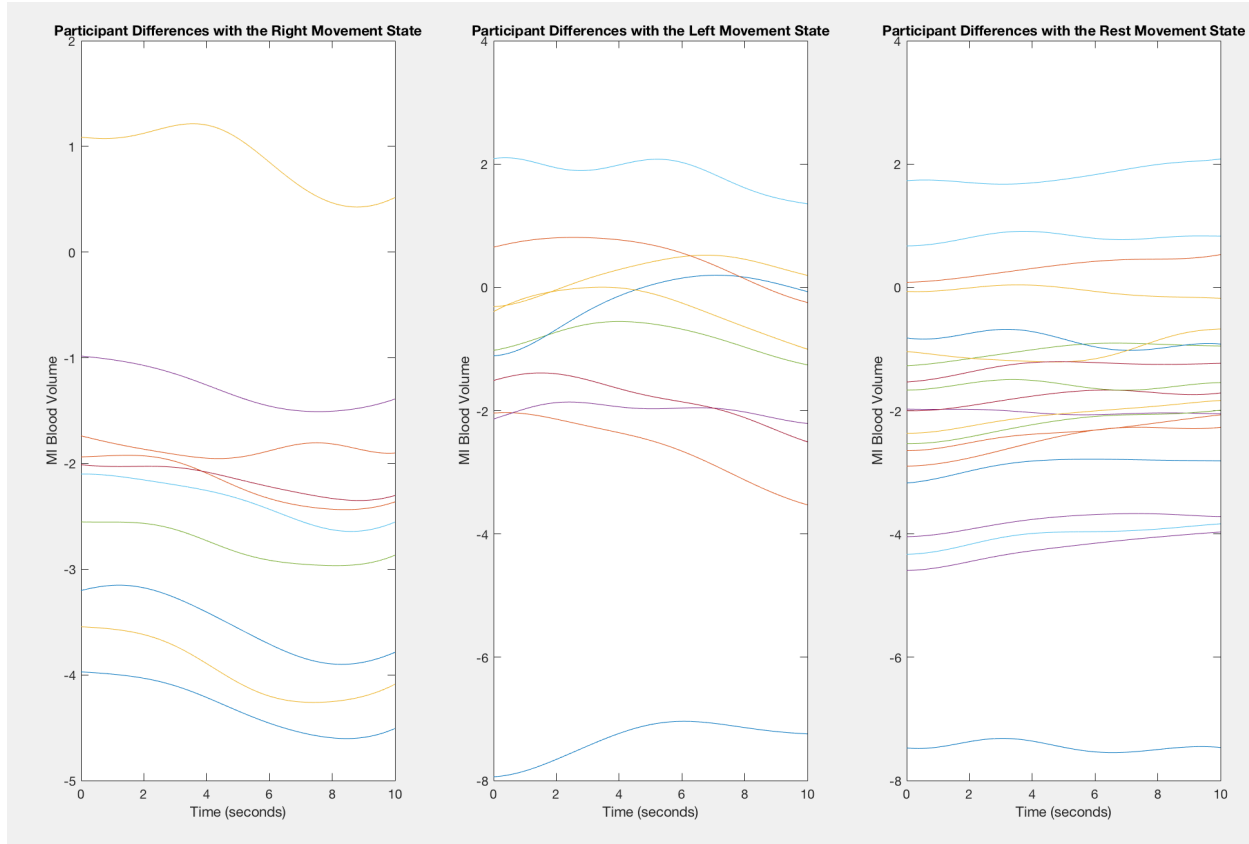


Figure 29: Filtered and Manipulated Motor Imagery Trial Blood Volume Data Averaged Epoch for the Relevant Channels Depicting the Difference Between Each Participant for Each State.

The following figure shows the motor imagery percentage of oxygenated hemoglobin concentration averaged epoch data for each of the right, left and rest states as a function of the difference between participant 1 and participant 2.

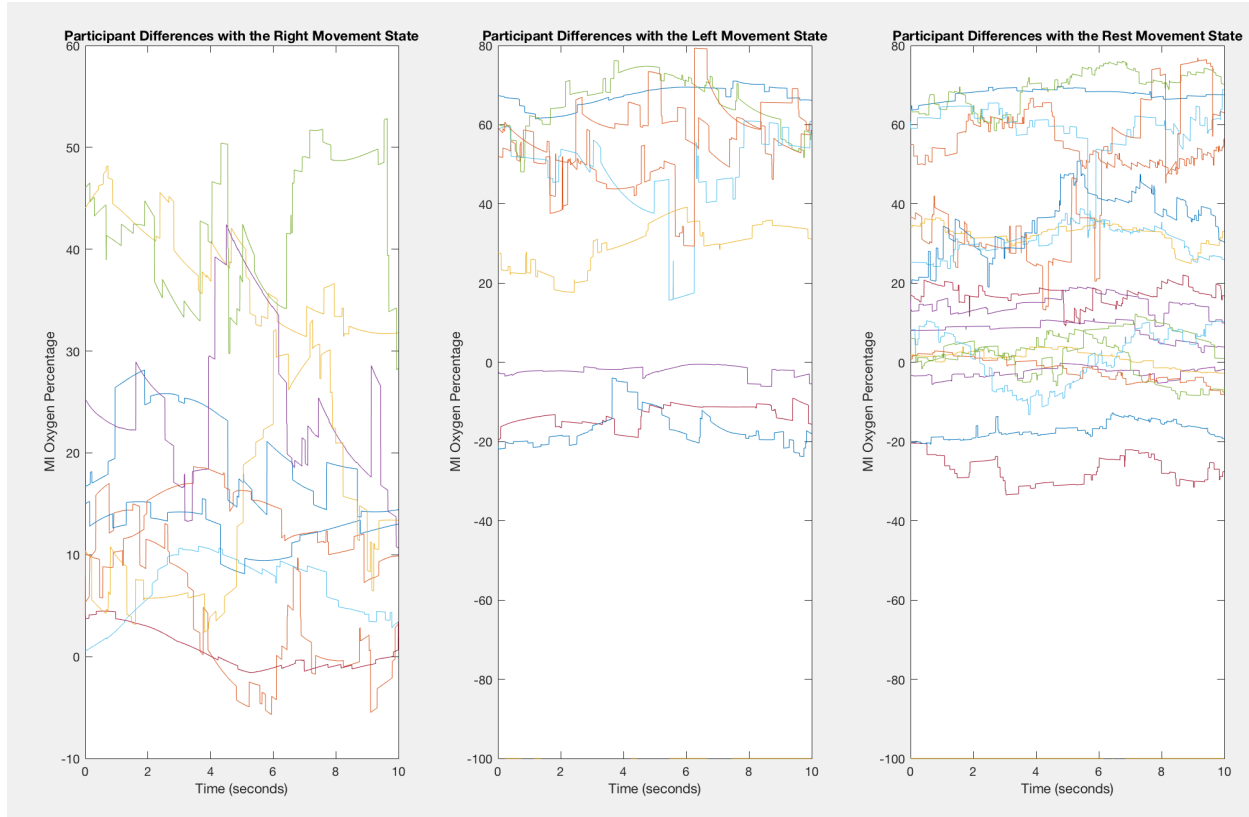


Figure 30: Filtered and Manipulated Motor Imagery Trial Percentage of Oxygenated Hemoglobin Data Averaged Epoch for the Relevant Channels Depicting the Difference Between Each Participant for Each State.

9.4. Static Blood Pressure Impact Analysis

The static blood pressure value calculated from average continuous blood pressure measurement during the calibration was compared using two datasets and was considered in terms of individual channels. In the below figures, each dataset is represented by the two participant datasets considered throughout this report. The following figures additionally include labels for the static blood pressure measured from each participant. With more collected data however, each dataset included in this section of analysis could represent the averaged epoch values for participants with each hypertensive and normal conditions so that the relationships between each considered variable and the measured static blood pressure could be considered.

The following figure displays the blood volume averaged epoch data for all considered participants as each individual relevant channel for the motor imagery rest state data.

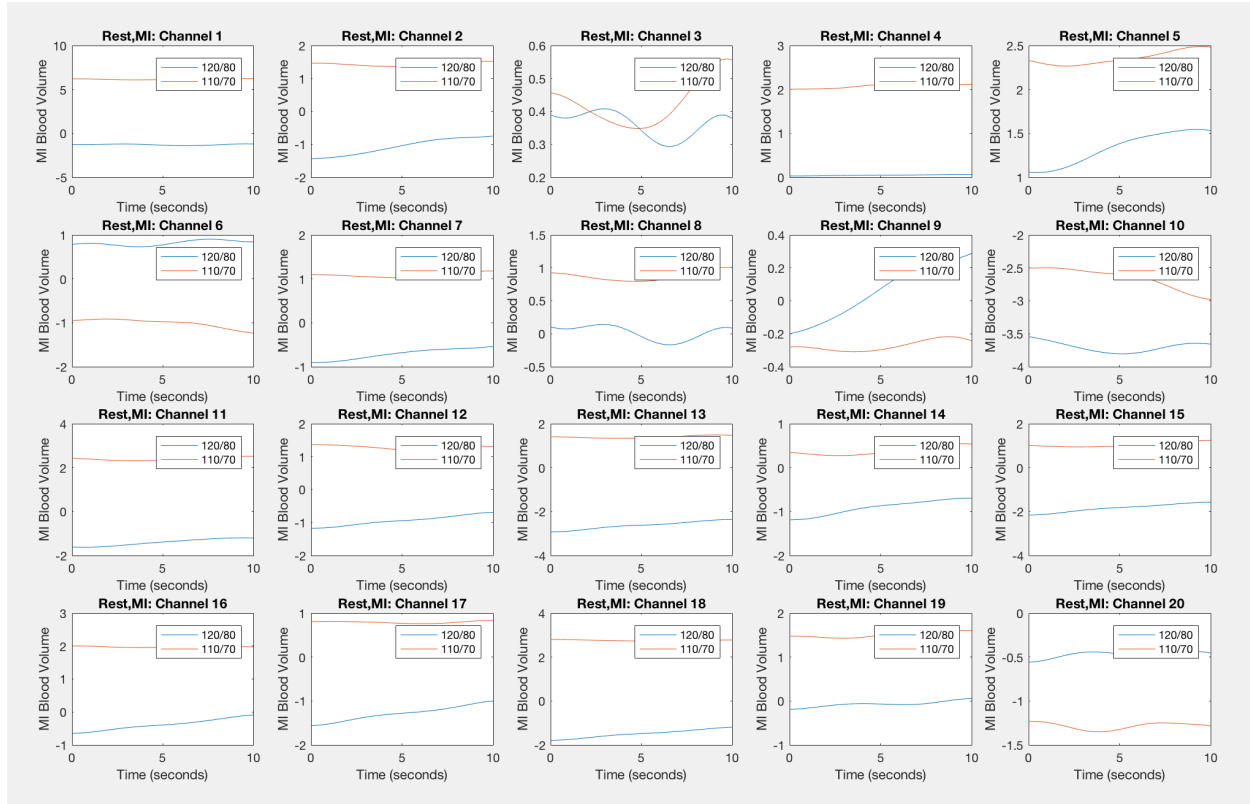


Figure 31: Filtered and Manipulated Motor Imagery Trial Blood Volume Data Averaged Epoch for Every Relevant Channel for the Rest State for Both Participants.

The following figure displays the blood volume averaged epoch data for all considered participants as each individual relevant channel for the motor imagery right state data.

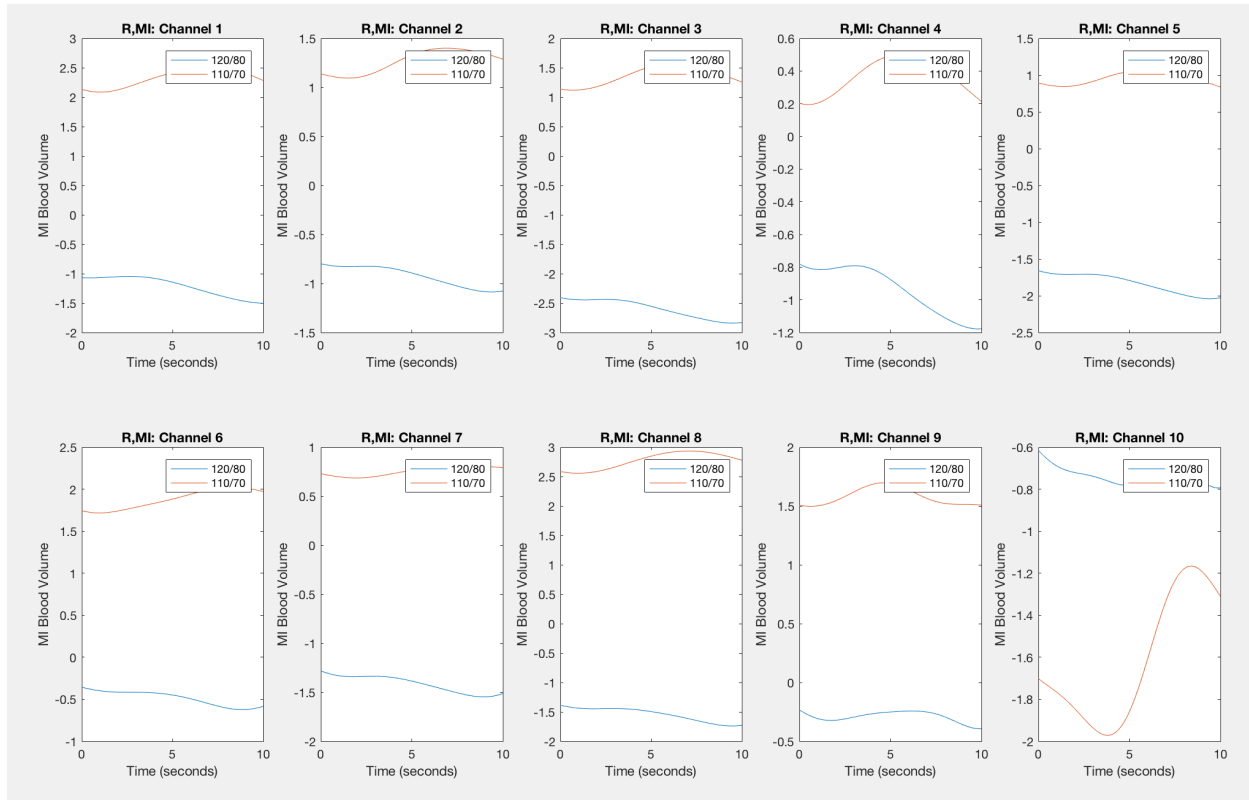


Figure 32: Filtered and Manipulated Motor Imagery Trial Blood Volume Data Averaged Epoch for Every Relevant Channel for the Right State for Both Participants.

The following figure displays the percentage of oxygenated hemoglobin concentration averaged epoch data for all considered participants as each individual relevant channel for the motor imagery rest state data.

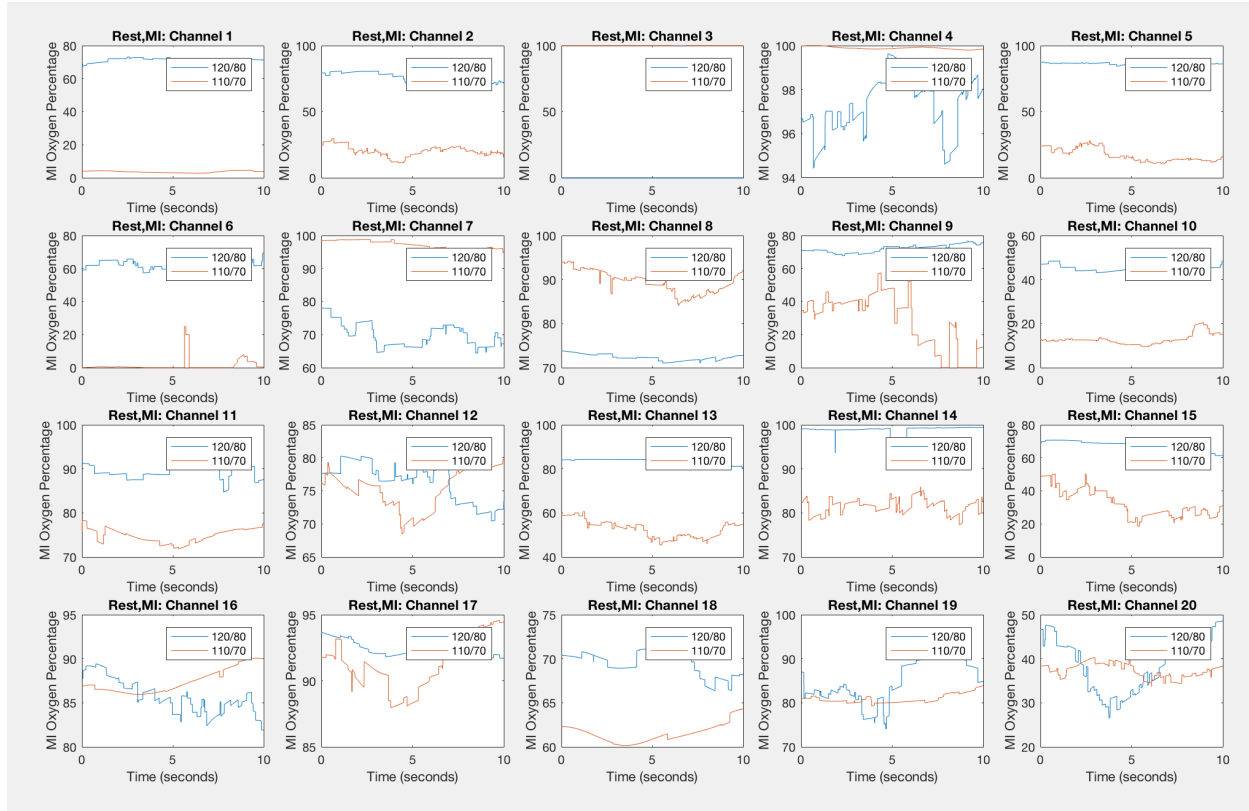


Figure 33: Filtered and Manipulated Motor Imagery Trial Percentage of Oxygenated Hemoglobin Data Averaged Epoch for Every Relevant Channel for the Rest State for Both Participants.

The following figure displays the percentage of oxygenated hemoglobin concentration averaged epoch data for all considered participants as each individual relevant channel for the motor imagery right state data.

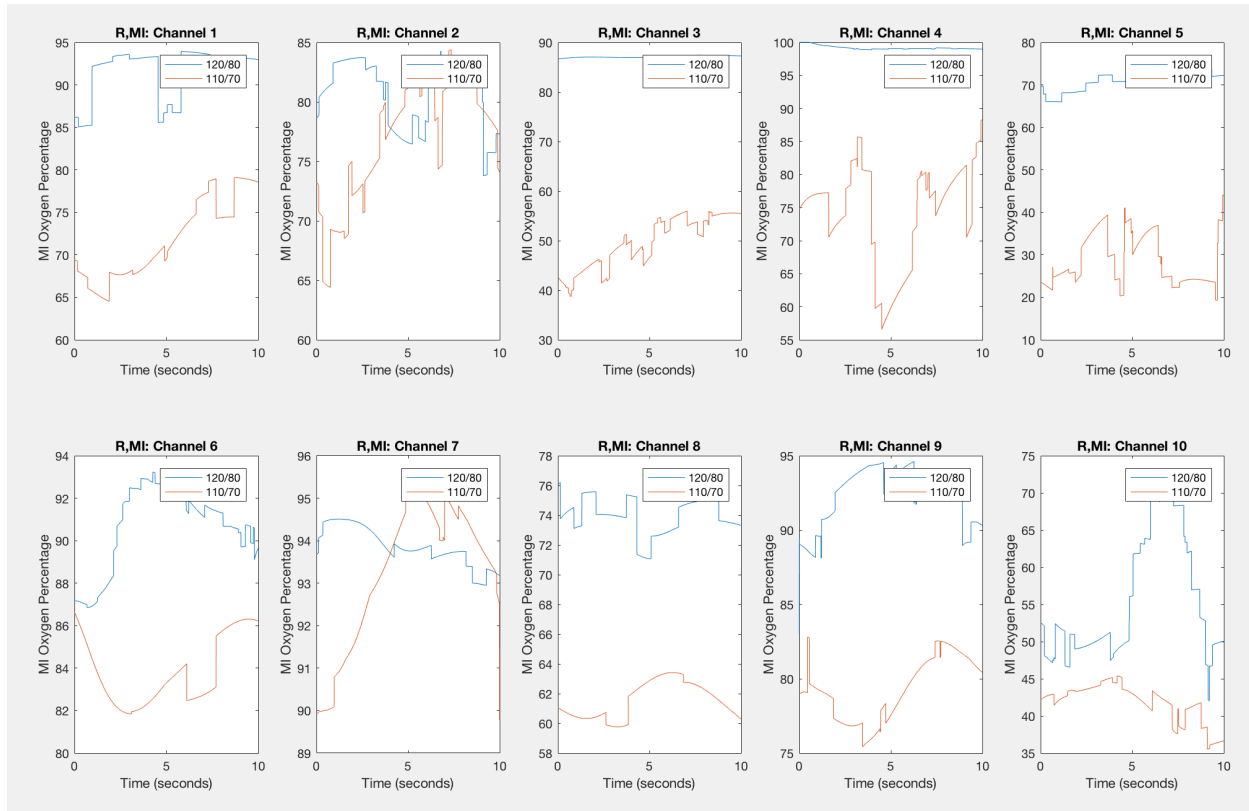


Figure 34: Filtered and Manipulated Motor Imagery Trial Percentage of Oxygenated Hemoglobin Data Averaged Epoch for Every Relevant Channel for the Right State for Both Participants.

9.5. Continuous Blood Pressure Trend Results

The trend analysis was conducted for the continuous blood pressure data by epoching and averaging the blood pressure data so that it can be compared to the fNIRS Data. Additionally, the overall trends of each stimulus were considered by averaging the averaged oxygen percentage epoch across all channels. The averaged epochs for the blood pressure data as well as the overall trend of each stimulus was considered and plotted below for the analysis of a potential relationship. If each of these trends calculated and summarized through an average for all participants with either hypertensive or normal blood pressure conditions the following figure would be very interesting to consider for relationships.

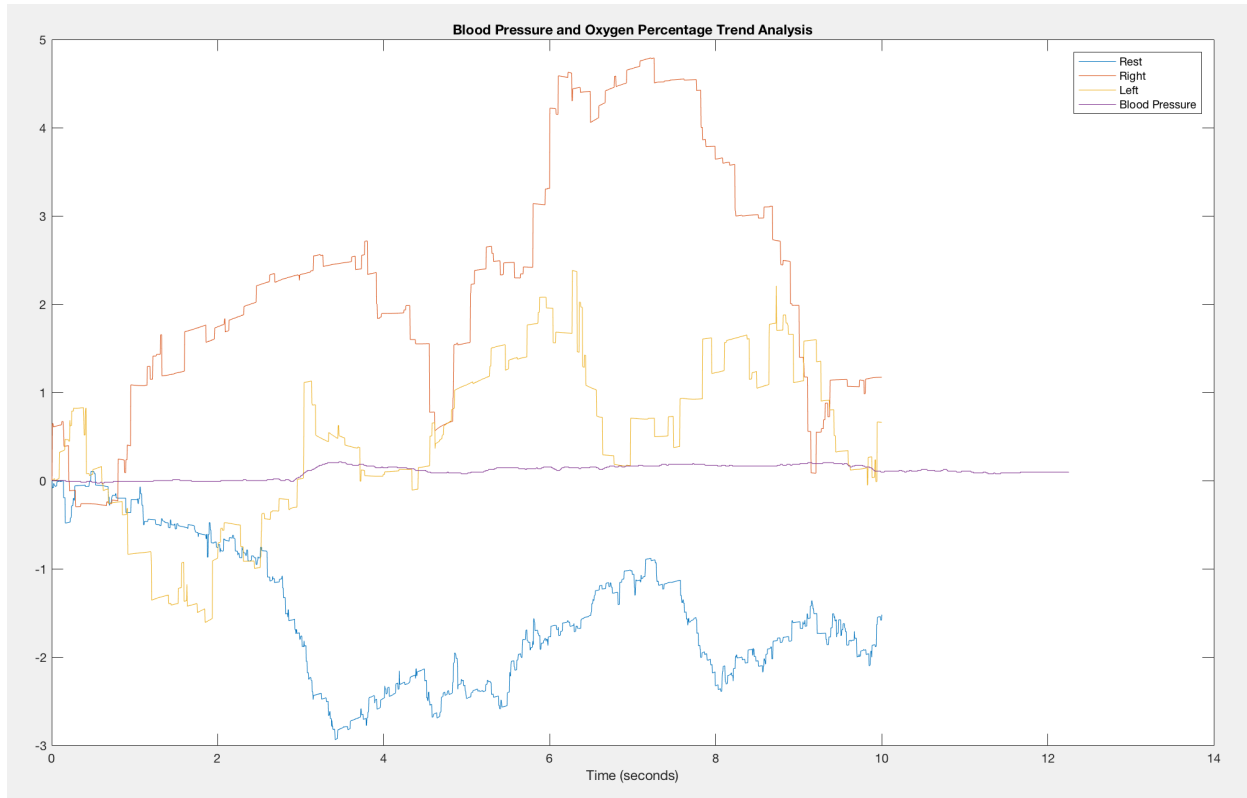


Figure 35: Participant 1 Motor Imagery Filtered and Manipulated Data for Summarized and Averaged Epochs for Percentage of Oxygenated Hemoglobin Concentration and Blood Pressure for Trend Analysis.

10.0. Theoretical and Empirical Comparison

The following theoretical model is not quantifiably directly comparable to the described empirical model as the two systems consider different variables. In particular, the theoretical and empirical models respectively consider wall shear stress and the oxygenated percentage of hemoglobin concentration. As these variables have a direct relationship however, trends simulated and empirically produced throughout this report can be directly compared through the graphs and qualitative relationships produced.

11.0. Acknowledgements

The research conducted and the software developed would not have been possible without the input, aid, and feedback of Dr. Claire Davies and PhD candidate Amir Moslehi. Additionally, the theoretical model was initiated in Dr. Rival's Biological Fluid Dynamics course and would not have been initiated without the information gained through this course and Dr. Rival's input at initial stages.

12.0. Conclusion

This project considered cutting edge research in the field of neuroscience and the fundamental principles of fluid dynamics to create a theoretical model and empirical experimental procedure and software to describe cerebral blood flow.

The theoretical model produced relationships that confirm that wall shear stress and therefore cell oxygenation, are greatly impacted by blood pressure. The basilar artery and the posterior cerebral artery produced more volatile

velocity fields, volumetric flow rates, and wall shear stress values throughout the cardiac cycle under hypertensive conditions. These results imply that brain activation changes under hypertensive conditions and may be similarly affected under other physiological conditions. Although the inaccuracies that come from a time-restricted crude model, such as created for this report, were present in the data, the results sufficiently confirm that the effect of fluid dynamics on cognitive functioning should be investigated more thoroughly. The effect of pressure changes on oxygen flux additionally confirms the hypothesis that neurological methods involving the measurement of brain activation through oxygen consumption must consider blood pressure and likely additional fluid properties as a relevant factor in analysis.

The designed empirical experiment and associated MATLAB software package was unable to reach conclusive relationships between the considered blood fluid dynamics properties due to incomplete data collection. The modular software package however was successfully completed and tested with collected data from two participants. This software package interprets and analyzes collected data and presents the qualitative and quantitative data in a comprehensible manner. Although the data collection and analysis were unable to reach completion within the timeframe of this project, the development of this package and the initial data collection comprised the majority of the required work for the research project.

Due to limited time and resources, the regional neural characteristics and properties and the highly scattering nature of neural tissue data recorded with fNIRS techniques were ignored [33] [34]. In future work on this research these factors should be considered. Additionally, not every potential metric from the collected data was calculated in the developed software. The signal processing of all data sets could be expanded to include more filtering on the data from each considered device. The fNIRS data analysis could be expanded to account for neural regions and the scattering nature of the tissue data. Finally, the calculated PPG metrics could be expanded to include quantified values for blood volume, oxygen saturation, blood pressure, and heart rate variability.

Moving forward, it is the intention that the research project be revisited to expand the dataset and further analyze the relationships between normal and hypertensive conditions in the motor imagery and motor execution experimental context.

Bibliography

- [1] World Health Organization, "Neurological Disorders and Public Health Challenges," World Health Organization, Geneva, Switzerland, 2006.
- [2] G. K. Jr, "Oxygen transport: interrelationship between arterial pressure regulation and blood flow autoregulation," *Medical Hypotheses*, vol. 36, no. 1, pp. 17-23, 1991.
- [3] R. S. Reneman and A. P. G. Hoeks, "Wall shear stress as measured in vivo: consequences for the design of the arterial system," *Medical and Biological Engineering and Computing*, vol. 46, no. 5, pp. 499-507, 2008.
- [4] B. PA, K. KK, D. TL, T. RB, W. EC, F. PT, B. JW, W. RM and R. BR., "Characterization of cerebral blood oxygenation and flow changes during prolonged brain activation," *US National Library of Medicine National Institutes of Health*, vol. 5, no. 2, pp. 93-109, 1997.
- [5] T. W. L. Scheeren, P. Schober and L. A. Schwarte, "Monitoring tissue oxygenation by near infrared spectroscopy (NIRS): background and current applications," *Journal of Clinical Monitoring and Computing*, vol. 26, no. 4, pp. 279-287, 2012.
- [6] NeurotechX, "Neurotech Edu Lessons: Introduction to BCI," 2019. [Online]. Available: <http://learn.neurotechedu.com/>. [Accessed 2019].
- [7] M. M. Laganà, S. J. Shepherd, P. Cecconia and C. B. Beggs, "Intracranial volumetric changes govern cerebrospinal fluid flow in the Aqueduct of Sylvius in healthy adults," *Biomedical Signal Processing and Control*, vol. 36, pp. 84-92, 2017.
- [8] B. v. d. Kolk, The Body Keeps the Score, Sept 25, 2015.
- [9] K.-S. Hong and N. Naseer, "FNIRS-based brain-computer interfaces: A review," *Frontiers in Human Neuroscience*, 2015.
- [10] D. A. Boas, C. E. Elwell, M. Ferrari and G. Taga, "Twenty years of functional near-infrared spectroscopy: introduction for the special issue," *NeuroImage*, no. 85, pp. 1-5, 2014.
- [11] G. Themelis, H. D'Arceuil and S. G. Diamo, "Near-infrared spectroscopy measurement of the pulsatile component of cerebral blood flow and volume from arterial oscillations," *J Biomed Opt.*, vol. 12, no. 1, 2007.
- [12] M. Elgendi, "On the Analysis of Fingertip Photoplethysmogram Signals," *Current Cardiology Reviews*, vol. 8, no. 1, pp. 14-25, 2012.
- [13] Leeds Beckett University, "Fluid flow in the brain unravelled for the first time," *Biomedical Signal Processing and Control*, 2017.
- [14] Rice University, "19.3 Cardiac Cycle," in *Anatomy and Physiology*, PressBooks, 2019.

- [15] Centers for Disease Control and Prevention, National Center for Health Statistics., "Underlying Cause of Death, 1999–2017," CDC WONDER Online Database: Centers for Disease Control and Prevention, Atlanta, GA, 2018.
- [16] Harvard University Medical School, "Men's Health: Blood pressure and your brain," 19 June 2019. [Online]. Available: <https://www.health.harvard.edu/heart-health/blood-pressure-and-your-brain>. [Accessed 10 March 2020].
- [17] P. RS and S. GD, "Increased peak blood velocity in association with elevated blood pressure.," *Ultrasound Medical Biology*, vol. 26, no. 9, pp. 1387-1391, 2000.
- [18] P. Slobodan Marinković M.D., M. M. M.D. and P. LasloPuškaš M.D., "Microvascular anatomy of the hippocampal formation," in *Surgical Neurology*, Institute of Anatomy, University Medical School, Belgrade, Yugoslavia, 1992, pp. 339-349.
- [19] Cutnell, J. & Johnson and Kenneth, Physics, Fourth Edition, Wiley, 1998: 308.
- [20] Engineering Toolbox, "Dynamic Viscosity of Common Liquids," 2008. [Online]. Available: https://www.engineeringtoolbox.com/absolute-viscosity-liquids-d_1259.html. [Accessed 2019].
- [21] W. C. H. P. a. S. J. L. H. Ha, "Effect of Swirling Blood Flow on Vortex Formation at Post-Stenosis," *Journal of Engineering in Medicine*, 2015.
- [22] N. L, N. H, C. D, R. RB and K. RA, "Age and sex differences in frontal lobe cerebral oxygenation in older adults-Normative values using novel, scalable technology: Findings from the Irish Longitudinal Study on Ageing (TILDA).," *Archives of Gerontology and Geriatrics*, 2019.
- [23] L. Couch, M. Roskosky, B. A. Freedman and M. S. Shuler, "Effect of Skin Pigmentation on Near Infrared Spectroscopy," *American Journal of Analytical Chemistry*, vol. 6, no. 12, pp. 911-916, 2015.
- [24] S. Wu, J. Li, L. Gao, C. Chen and S. He, "Suppressing Systemic Interference in fNIRS Monitoring of the Hemodynamic Cortical Response to Motor Execution and Imagery," *Frontiers of Human Neuroscience*, vol. 12, no. 85, 2018.
- [25] L. Minati, I. U. Kress, E. Visani, N. Medford and H. D. Critchley, "Intra- and extra-cranial effects of transient blood pressure changes on brain near-infrared spectroscopy (NIRS) measurements," *Journal of Neuroscience Methods*, vol. 197, no. 2, pp. 283-288, 2011.
- [26] Y. Ma, J. Choi, A. Hourlier-Fargette, Y. Xue, H. U. Chung, J. Y. Lee, X. Wang, Z. Xie, D. Kang, H. Wang, S. Han, S.-K. Kang, Y. Kang, X. Yu, M. J. Slepian, M. S. Raj and e. al., "Relation between blood pressure and pulse wave velocity for human arteries," *PNAS*, vol. 115, no. 44, pp. 11144-11149, October 2018.
- [27] T. Y. Abay and P. A. Kyriacou, "Photoplethysmography for blood volumes and oxygenation changes during intermittent vascular occlusions," *Journal of Clinical Monitoring and Computing*, vol. 32, no. 3, pp. 447-455, 2018.

- [28] M. Elgendi, R. Fletcher, Y. Liang, N. H. L. Newton Howard, D. Abbott, K. Lim and R. Ward, "The use of photoplethysmography for assessing hypertension," *NPJ Digital Medicine*, vol. 2, no. 60, 2019.
- [29] M. D. Pfeifer, F. Scholkmann and R. Labruyère, "Signal Processing in Functional Near-Infrared Spectroscopy (fNIRS): Methodological Differences Lead to Different Statistical Results," *Frontiers in Human Neuroscience*, 2019.
- [30] K. L.M.Koenraadt, E. G. Roelofsen, J. Duysens and N. L.W.Keijsersa, "Cortical control of normal gait and precision stepping: An fNIRS study," *Elsevier*, vol. 85 Part 1, pp. 415-422, 2014.
- [31] D. Castaneda, A. Esparza, M. Ghamari, C. Soltanpur and H. Nazeran, "A review on wearable photoplethysmography sensors and their potential future applications in health care," *International Journal on Biosensors and Bioelectronics*, vol. 4, no. 4, pp. 195-202, 2018.
- [32] Y. K. Qawqzeh, R. Uldis and M. Alharbi, "Photoplethysmogram second derivative review: Analysis and applications," *Scientific Research and Essays*, vol. 10, no. 21, pp. 633-639, 2015.
- [33] C. AM, F. MA, T. CH, L. KA, M. EL, Z. B, K. T, G. A, G. G and F. M, "Individual differences in regional cortical volumes across the life span are associated with regional optical measures of arterial elasticity.," *NeuroImage*, no. 162, pp. 199-213, 2017.
- [34] M. Cope, D. T. Delpy, E. O. R. Reynolds, S. Wray, J. Wyatt and P. v. d. Zee, "Methods of Quantitating Cerebral Near Infrared Spectroscopy Data," in *Advances in Experimental Medicine and Biology*, London, Department of Medical Physics and Bio-Engineering, University College London, 1988, pp. 183-189.
- [35] A. Mehinovic, E. Isakovic and J. Delic, "Variations in Diameters of Vertebro-basilar Tree in Patients with or with No Aneurysm," *US National Library of Medicine National Institutes of Health*, vol. 68, no. 1, pp. 27-29, 20 February 2014.
- [36] A. P. a. N. Fatourae, "An analytical phantom for the evaluation of medical flow imaging algorithms," *Phys. Med. Biol.*, vol. 54, p. 1791–1821, 2009.
- [37] M. D. Pfeifer, F. Scholkmann and R. Labruyère, "Signal Processing in Functional Near-Infrared Spectroscopy (fNIRS): Methodological Differences Lead to Different Statistical Results," *Frontiers in Human Neuroscience*, 2018.

Appendix A: Theoretical Methods and Model

Model Specifications

This model was designed to analyze changes in the wall shear stress of blood vessels throughout the cardiac cycle.

The following Fourier analysis and flow dynamics were calculated using a published arterial analysis developed for cardiac research [33]. The equations used throughout analysis can be seen in detail in the model, which is publicly posted under the Github repository abbyholland/neural_fluid_dynamics. Additionally, the model components which rely on previously developed functions can also be seen in this Github repository with the initial publishing licenses included.

A Fourier analysis was conducted to describe the discrete pressure values as a temporal wave. This analysis was initially conducted by setting variables p_0 , A, and B as values in a wave function.

$$p_0 = p_0 + \text{pressure}(t) * \frac{dt}{T} \quad (1)$$

$$A(t) = A(t) + 2 * p(n) * \cos \cos (2 * \pi * t(n)) * \frac{dt}{T} \quad (2)$$

$$B(t) = B(t) + 2 * p(n) * \sin \sin (2 * \pi * t(n)) * \frac{dt}{T} \quad (3)$$

These values produced for A and B are then used to define p_n and phi, as shown in the following equation:

$$p_n(n) = \sqrt{A(n)^2 + B(n)^2} \quad (4)$$

$$\text{phi}(n) = \text{angle_of}(A(n) + i * B(n)) \quad (5)$$

The conducted Fourier analysis takes discrete pressure values and generates coefficients p_0 , p_n , and phi to describe the following temporal pulsatile wave pressure function:

$$p(t) = p_0 + \text{sum} \left(p_n(n) * e^{i * \left(\frac{2 * \pi * t * n}{T - \varphi(n)} \right)} \right) \quad (6)$$

The coefficient p_0 represents the steady state component of the periodic wave. The produced values of p_n and phi respectively represent the absolute values and phase angle of the produced Fourier series. The value n represents the number of coefficients produced in the Fourier function, t represents the time value of the function, and T represents the period of the function.

These produced Fourier coefficients (p_0 , p_n , and phi), the artery radius, the dynamic viscosity (μ) and the density of blood (ρ) were used in flow calculations.

The Bessel function was computed with variations of kapa as the Z input value, as defined below. In this equation, ρ is density and μ is kinematic viscosity.

$$\text{kapa} = \left(\text{radius} * \sqrt{2 * \pi * \text{frequency} * \frac{\rho}{\mu}} \right) * i^{1.5} / \text{radius} \quad (7)$$

Flow Properties

The calculations used in this model were largely derived from the below incompressible continuity and the Navier-Stokes equation in a cylindrical coordinate system. These equations were manipulated using the boundary

conditions and the Bessel function to produce the pressure (p), wall shear stress (τ), and volumetric flow (q) for each time step. Each calculation derivation can be seen in the cardiac research article produced by A Pashaei and N Fatouraee for the Biomedical Engineering Faculty at Tehran Polytechnic [33].

$$\nabla \cdot u = 0 \quad (8)$$

$$\frac{1}{\rho} \nabla p = \frac{\mu}{\rho} \nabla^2 u - u \cdot \nabla u - \frac{\partial u}{\partial t} \quad \nabla \cdot u = 0 \quad \rho \frac{\partial w}{\partial t} = -\frac{\partial p}{\partial z} + \mu \left(\frac{\partial^2 w}{\partial^2 r} + \frac{1}{r} \frac{\partial w}{\partial r} \right) \quad (9)$$

The pressure was calculated as a function of time using the p_n absolute value and the phi value produced from the Fourier analysis and the following equation:

$$p(t) = p_n(n) * e^{i*(2*\pi*frequency*t*n-\varphi(n))} \quad (10)$$

The shear stress applied to the arterial wall was calculated using two Bessel functions with Z value inputs of $kappa*radius$ (producing Bessel1) and $kappa*0.93*radius$ (producing Bessel2), respectively. The wall shear stress was then found using the following general shear stress equation in the coordinate system {r, z, w}:

$$\tau_{rz} = -\mu \left(\frac{\partial w}{\partial r} - \frac{w}{r} \right) \quad (11)$$

Under the circumstances presented for this model, the general shear stress equation above is derived to become the following equation:

$$\tau(t) = \frac{(-\mu * p_0 * radius * 0.93) * \mu}{2} + real_component \left(\frac{i * kappa * omega}{\rho * n + (\frac{n+1}{2})} * \frac{Bessel1}{Bessel2} * p(t) \right) \quad (12)$$

The volumetric flow rate q is derived from the following general equation.

$$q = \int_0^{radius} 2 * \pi * r * w * dr \quad (13)$$

The above equation was used to derive the volumetric flow of blood through each blood vessel:

$$q(t) = \frac{p_0 * \pi * \left(\frac{(radius * 0.93)^4}{2} - r^2 * (radius * 0.93)^2 \right) * \mu}{4} + real_component \left(\frac{i * 2 * \pi * (2 * \pi * frequency)}{\rho * (n + \frac{n+1}{2})} * \frac{(radius * 0.93)^2}{2} - \frac{radius * 0.93 * Bessel1 * kappa}{Bessel2} * p(t) \right) \quad (14)$$

Velocity Calculations

When calculating velocity the Bessel function was computed using a Z value of both $kappa*radius$ (producing Bessel3) and $kappa*h*ri$ (producing Bessel4) where ri is radius at each x and y value, and h is the radial distance away from the centerline of the artery.

The velocity is calculated at each dimension and timestep using the below equations. The produced matrix includes a 2-Dimensional (x,y) velocity field at each timestep.

$$u(t, x, y) = \frac{p_0 * ((ri * h)^2 - r^2) * \mu}{4} + real_component_of \left(\frac{i * 2 * \pi * f}{\rho * (n * \frac{n+1}{2})} * \left(1 - \frac{Bessel4}{Bessel3} \right) * p(t) \right) \quad (15)$$

Appendix B: Additional Graphs

fNIRS Averaged Values

The following figure shows the average concentration of oxygenated hemoglobin for participant 1's motor imagery experiments in the 10 seconds following each stimulus. The relevant channels for the three stimuli are presented side-by-side for qualitative comparative trend analysis.

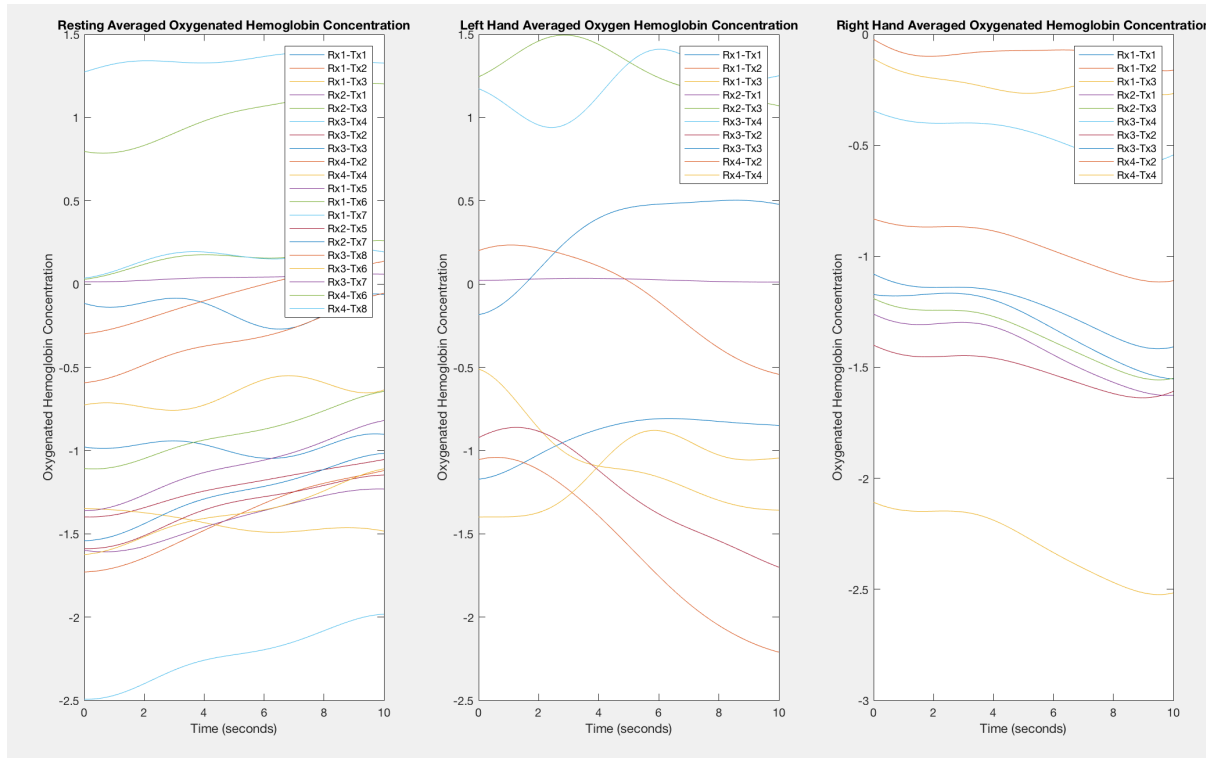


Figure 36: Participant 1 Motor Imagery Filtered and Manipulated Data Depicting the Averaged Epoch for Oxygenated Hemoglobin Concentration for the Relevant Channels of each State: Rest, Right, and Left.

The following figure shows the average concentration of deoxygenated hemoglobin for participant 1's motor imagery experiments in the 10 seconds following each stimulus. The relevant channels for the three stimuli are presented side-by-side for qualitative comparative trend analysis.

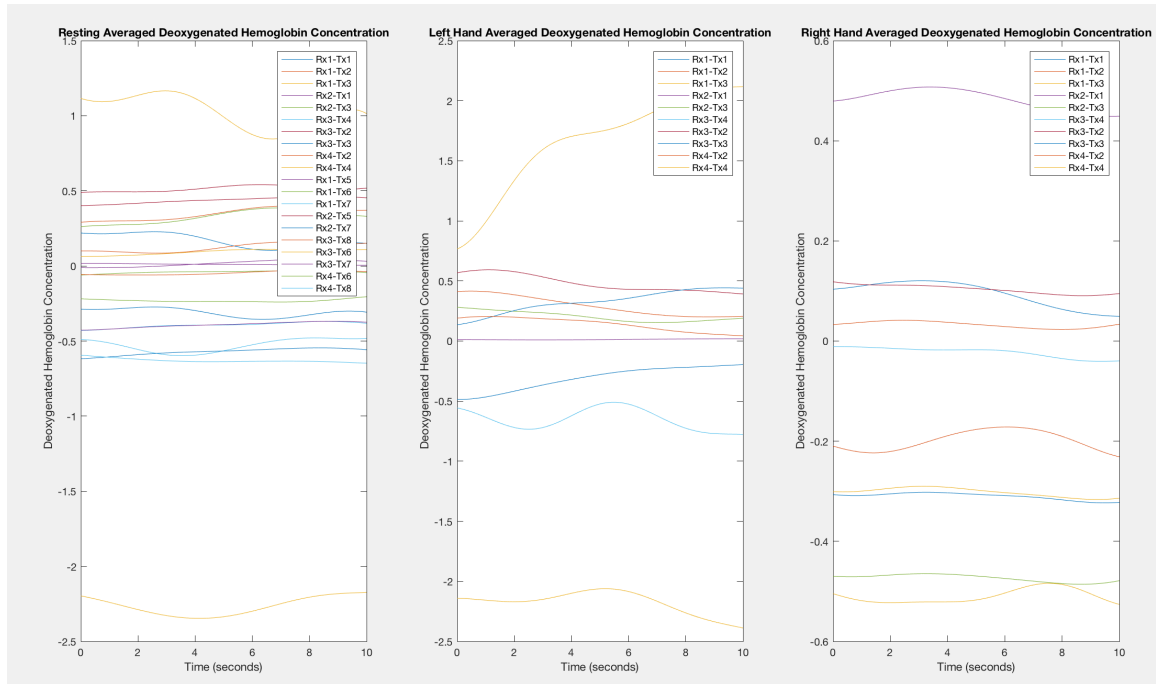


Figure 37: Participant 1 Motor Imagery Filtered and Manipulated Data Depicting the Averaged Epoch for Deoxygenated Hemoglobin Concentration for the Relevant Channels of each State: Rest, Right, and Left.

Action Comparison Analysis

The additional graphs calculated for the Action Comparison Analysis can be seen below.

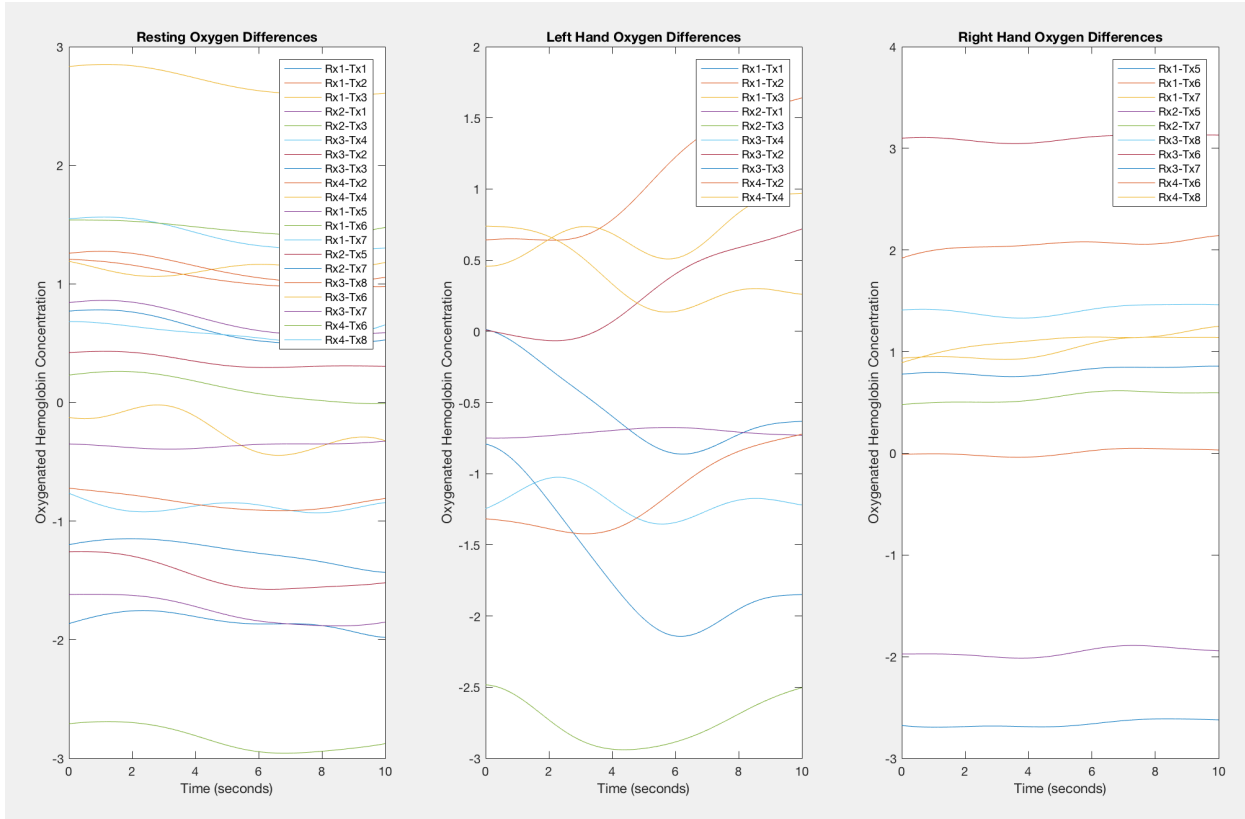


Figure 38: Participant 1 Filtered and Manipulated Averaged Oxygenated Hemoglobin Concentration Epoch for the Relevant Channels of the Differences between the Motor Imagery and Motor Execution Data for Each State.

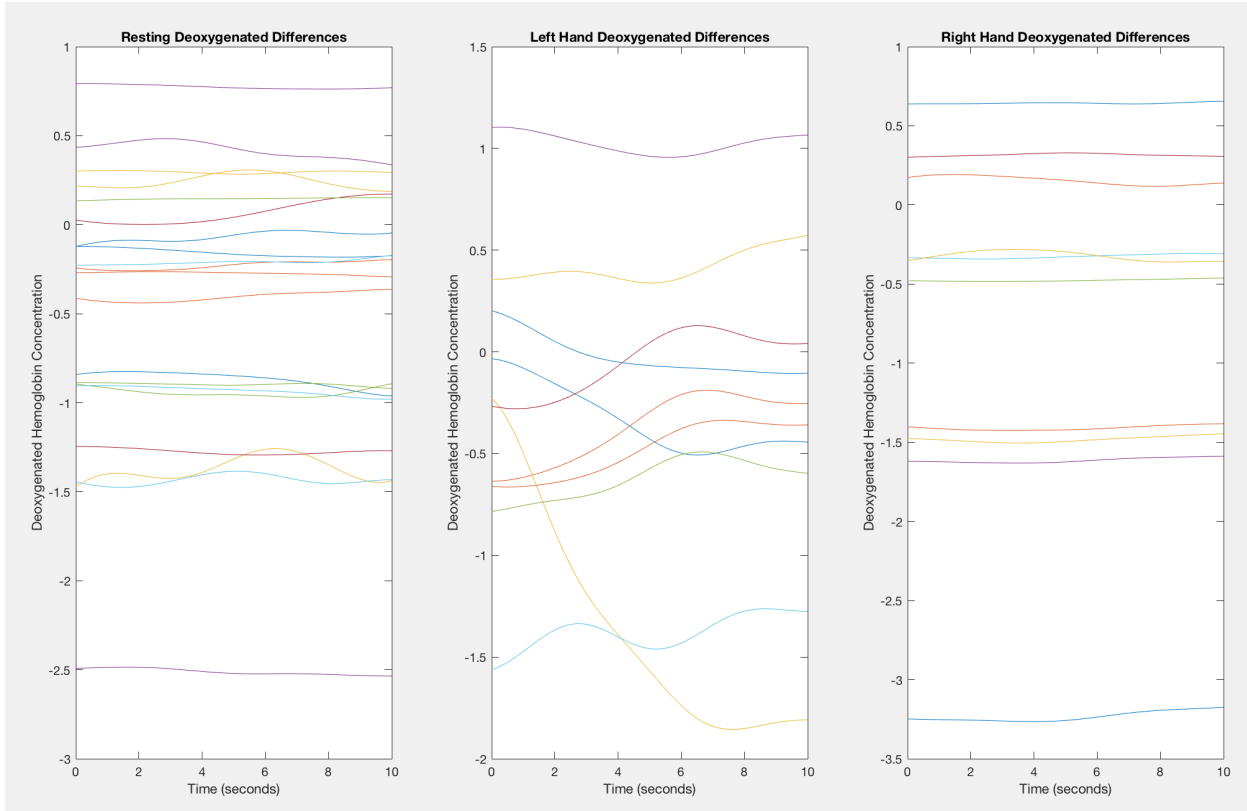


Figure 39: Participant 1 Filtered and Manipulated Averaged Deoxygenated Hemoglobin Concentration Epoch for the Relevant Channels of the Differences between the Motor Imagery and Motor Execution Data for Each State.

Static Blood Pressure Impact Analysis

The additional graphs calculated for each channel for the Static Blood Pressure Impact Analysis can be seen below.

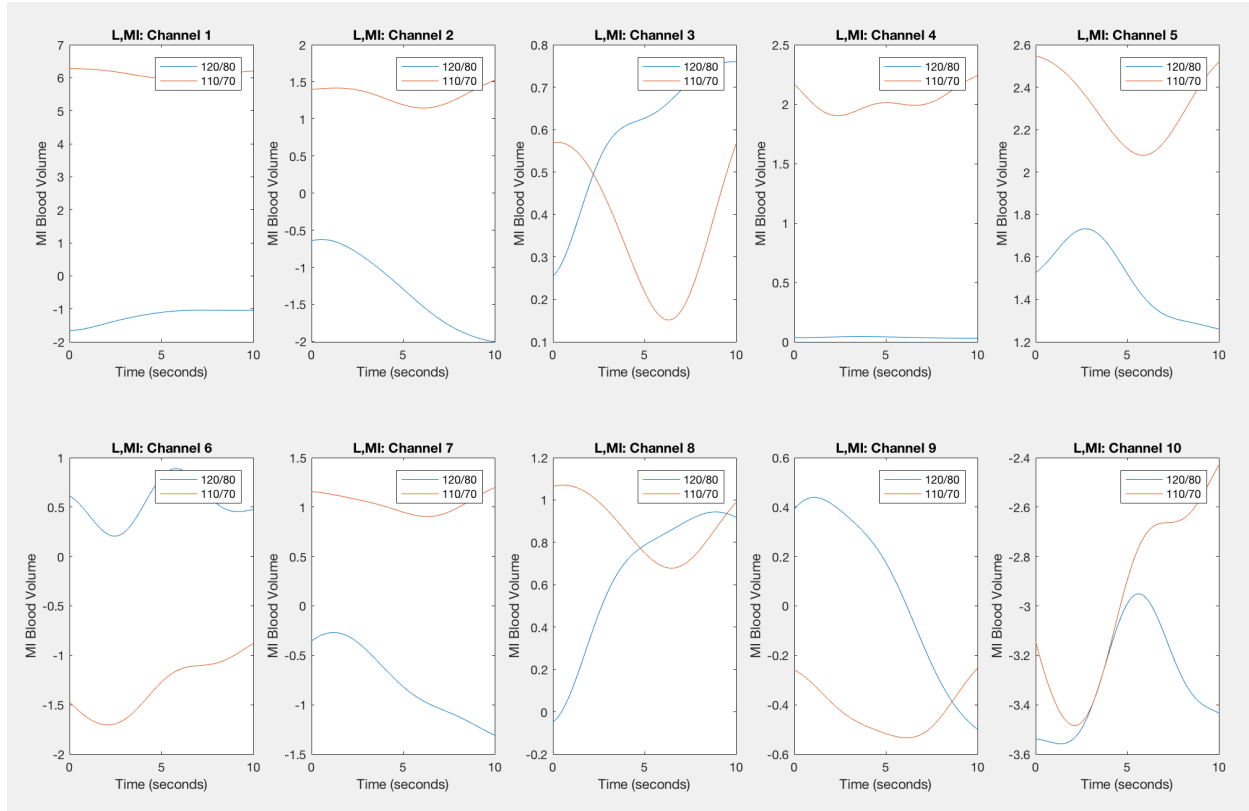


Figure 40: Filtered and Manipulated Motor Imagery Trial Blood Volume Data Averaged Epoch for Every Relevant Channel for the Left State for Both Participants.

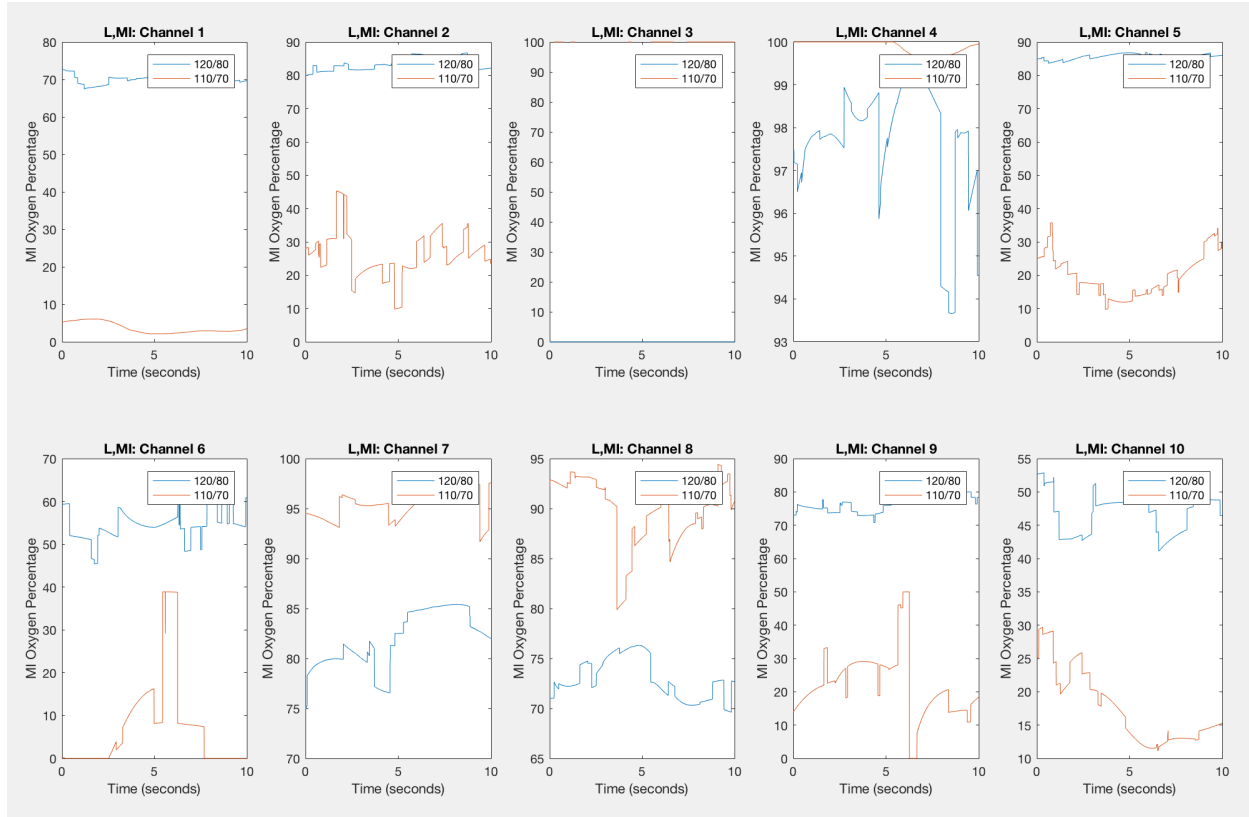


Figure 41: Filtered and Manipulated Motor Imagery Trial Percentage of Oxygenated Hemoglobin Data Averaged Epoch for Every Relevant Channel for the Left State for Both Participants.